Chemical Geology 631 (2023) 121503

Contents lists available at ScienceDirect

Chemical Geology

journal homepage: www.elsevier.com/locate/chemgeo

C–O–H fluid-melt-rock interaction in graphitic granulites and problems of quantifying carbon budget in the lower continental crust

Bruna B. Carvalho *, Omar Bartoli, Bernardo Cesare

Dipartimento di Geoscienze, Università degli Studi di Padova, Via G. Gradenigo 6, Padova 35131, Italy

ARTICLE INFO

Editor: Balz Kamber

Keywords:
Carbon budget
Lower continental crust
C–O–H fluids
Graphite-bearing granulite
Fluid-melt immiscibility

ABSTRACT

Estimates on the geological carbon cycle are subject to large uncertainties that can be reduced by thorough observation of rocks. In this contribution, we focus specifically on C–O–H fluid-melt-rock interactions in graphitic metapelitic granulites and on their bearing to the carbon budget of granulitic roots of continents. We provide robust microstructural and thermometric constraints on the coexistence of anatectic silicate melts and C–O–H fluids up to near ultrahigh temperature conditions in the archetypal crustal section of Ivrea-Verbano Zone (IVZ, Italian Alps). Fluid inclusions in garnet are investigated before and after high-temperature experiments, and contain considerable proportions of CO_2, CH_4, N_2, but lower H_2O than predicted for graphitic systems at granulite facies. When comparing and contrasting the melt compositions obtained by Perple_X and rhyolite-MELTS with natural melts from IVZ, a much better match is obtained by the former, questioning the choice of rhyolite-MELTS for modelling melting equilibria of metasedimentary rocks and for quantifying carbon budget of the lower crust. Overall, data show that assuming only a limited extent of fluid-melt immiscibility in the deep crust contradicts the evidence from natural rocks and prompts to an incomplete view of actual carbon behavior and carbonic fluids. The available experimental dataset on CO_2 solubility in felsic melts cannot be used to interpret the volatile budget of melt inclusions in graphitic migmatites and granulites, as most solubility experiments were conducted under carbonate-saturated (i.e. highly oxidizing) conditions which maximize CO_2 content of melt, compared to graphitic (i.e. more reducing) protoliths. As a consequence, thermodynamic models still cannot account for all the complexities related with interactions among H_2O–CO_2–CH_4 ternary fluids, H_2O- and CO_2-bearing anatectic melts and graphite-bearing residues in graphitic metapelites. Targeted experimental studies are therefore crucial to boost substantial computational efforts, before any precise estimates on carbon budget and fluxes in the lower anatectic crust can be made.

1. Introduction

The carbon cycle operates over millions of years and involves slow exchange between rocks and superficial systems. In the last decade, many efforts have focused on quantifying carbon fluxes among distinct geological reservoirs (e.g. Dasgupta and Hirschmann, 2010; Kelemen and Manning, 2015; Stewart and Ague, 2020). The principal mechanism of input of carbon to the Earth's interior is thought to occur in subduction zones (Plank and Manning, 2019), where carbonates and organic carbon are carried at depth, and decarbonation, dissolution and melting reactions may release carbon-bearing fluids and melts to the mantle wedge (e.g. Frezzotti et al., 2011; Ague and Nicolescu, 2014; Poli, 2015; Vitale Brovarone et al., 2017; Martin and Hermann, 2018; Stewart and Ague, 2020). Additionally, part of the subducted crustal carbon may reach lower mantle depths and form diamonds (Nestola et al., 2018). However, quantifying the long-term geological carbon cycle is still in its infancy owing to the large extrapolations from models. The most significant uncertainties regard: i) the nature of the interactions between fluids, melts and rocks and their effect on carbon mobility (e.g. Tumiati et al., 2017; Guo et al., 2022), ii) the reliability of extrapolating scattered field-based observations or analogue models from experiments to the large-scale natural carbon cycling (e.g. Epstein et al., 2020; Scambelluri et al., 2022) and iii) the existence of potential contributors which are commonly overlooked – i.e., collisional orogenic settings (Groppo et al., 2022).

Regarding the last point, the paradigm of a mafic deep continental crust (Rudnick and Fountain, 1995) has been challenged and more felsic, metasedimentary rocks are considered an important, sometimes

* Corresponding author.
E-mail address: bruna.borgescarvalho@unipd.it (B.B. Carvalho).

https://doi.org/10.1016/j.chemgeo.2023.121503
Received 13 December 2022; Received in revised form 17 April 2023; Accepted 18 April 2023
Available online 23 April 2023

predominant, component (Ferri et al., 2013; Hacker et al., 2015; Wang et al., 2021). Carbonate rich rocks (marbles and calcsilicates) represent important carbon hosts in metasedimentary sequences. In addition, most granulite-facies felsic rocks in orogenic belts contain graphite (Huizenga and Touret, 2012) and laboratory measurements demonstrated that residual graphitic metapelitic granulites show seismic signatures very similar to those of mafic granulites (Ferri et al., 2016). Therefore, anatexis of graphitic metapelites in roots of continents and extraction of anatectic melts may contribute to the geological carbon cycle globally. However, our understanding of carbon budget during melting of graphitic metapelites is still limited. Recently, Nicoli et al. (2022) attempted to quantify the flux of carbon related to the burial of siliciclastic sediments in the lower orogenic crust (0.2–4.4 Mt. C/yr) and the volume of carbon lost by extraction of anatectic magmas (0.18–3.8 Mt. C/yr). Their computational and quantitative effort was based on recent findings of nanogranitoids (NGs; i.e. former melt inclusions) and carbonate- and CO_2-bearing multiphase fluid inclusions (MFI) coexisting in peritectic garnet of many high-grade metamorphic terranes and representing one of the most solid lines of evidence for carbon mobility during high-grade metamorphism and anatexis (Carvalho et al., 2020 and references therein). Taking as case study the crustal section of the Ivrea-Verbano Zone (IVZ, Italian Alps), where NGs and MFI coexist in the same clusters reflecting conditions of melt-fluid immiscibility, the work of Nicoli et al. (2022) by means of rhyolite-MELTS software (Gualda et al., 2012) suggested that the coexistence of anatectic melts and C–O–H fluids in the graphite-bearing deep crust must occur only during the early stages of partial melting (at 700–750 °C). According to their results, C–O–H fluids should disappear at higher temperatures as they should partition into the melt. As a consequence, only a carbon-bearing anatectic melt would be present in granulitic roots of continents. However, this view is in conflict with microstructural and thermometric constraints, which instead support the persistence of C–O–H fluids with anatectic melts at considerably warmer conditions in Earth's continental crust (Carvalho et al., 2019, 2020).

Understanding whether or not C–O–H fluids may persist during anatexis up to high temperature (HT) or even ultrahigh temperature (UHT) conditions (i.e. >900 °C) is of utter importance, because the occurrence of carbon-bearing fluids has broad implications for the fluid regime and melt productivity of the deep crust (Johannes and Holtz, 1990), the rheology of the lithosphere (Gerya and Meilick, 2011) and the geological carbon cycle (Chu and Ague, 2013). The main aims of this contribution are to i) document step by step robust lines of evidence supporting C–O–H fluid persistence up to HT and near UHT conditions in the IVZ graphitic deep crust, ii) investigate the composition of fluids in graphitic granulites from IVZ, iii) compare and contrast the results of different approaches of software packages to evaluate their reliability to reproduce compositions of anatectic melts from metapelites, iv) critically assess the existing experimental dataset of CO_2 solubility in rhyolitic melts, and v) propose some directions for future studies on carbon budget of the deep anatectic crust.

2. CO_2 and granulites

CO_2-bearing fluid inclusions found in granulites have been considered the main advocate for an active role of fluids during HT and UHT metamorphism (Newton et al., 1980b; Touret, 1971; Touret and Huizenga, 2012). However, since the majority of past studies investigated fluid inclusions in quartz and/or did not report clear textural evidence of their primary nature (e.g. Touret, 1971; Van den Kerkhof and Olsen, 1990; Sarkar et al., 2003), the high-temperature origin of such CO_2 still remains controversial (e.g., Harley, 2004; Cesare et al., 2005), and CO_2-bearing fluids are still not generally considered to play an active major role during anatexis (Brown, 2013). Rather, they could be a necessary consequence of fluid-melt partitioning of volatile species at high-temperature, H_2O being much more soluble than CO_2 in the silicate melt (Tamic et al., 2001; Behrens et al., 2004).

However, when primary melt and CO_2-bearing fluid inclusions are found in same clusters within peritectic minerals (e.g., garnet, cordierite, spinel), which are by definition the solid products of incongruent melting reactions, these findings indisputably prove the existence of CO_2-bearing fluids during prograde metamorphism and anatexis (Cesare et al., 2007; Ferrero et al., 2011; Carvalho et al., 2020; Bartoli, 2021; Bartoli and Cesare, 2020; and references therein). As result of the continuous effort on the thorough investigation of melt inclusions in high-grade rocks, several case studies demonstrated that CO_2-bearing fluid inclusions often coexist with anatectic melt in the same clusters of peritectic garnet (e.g. Cesare et al., 2007; Barich et al., 2014; Ferrero et al., 2011, 2014, 2019; Tacchetto et al., 2019; Carvalho et al., 2019, 2020; Gianola et al., 2021; Ferri et al., 2020; Safonov et al., 2020). Many of these studies deal with graphite-bearing anatectic rocks. Such findings strongly indicate that fluid-melt immiscibility at suprasolidus conditions may not be as rare as expected and that C–O–H fluid-present melting of the deep continental seems to represent an important petrogenetic process of crustal magmas, provided that their occurrence up to UHT conditions is well constrained.

3. Geological and petrological background

The Ivrea Verbano Zone (NW Italy) is a preserved section of mid to lower Carboniferous-Permian continental crust tilted and faulted by Alpine tectonics (Schmid and Wood, 1976; Bea and Montero, 1999). The IVZ is composed of ultramafic rocks (Balmuccia and Finero peridotites), mafic rocks of the Mafic Complex and the supracrustal rocks of the Kinzigite Formation (Quick et al., 2003). The Kinzigite Formation comprises abundant graphitic metapelites interlayered with metagreywackes, metabasites, and subordinate marbles, calcsilicates and quartzites (Schmid, 1993). The whole supracrustal sequence shows an increase in metamorphic grade from amphibolite facies in the SE to granulite facies in the NW (Schmid, 1993; Redler et al., 2012, 2013; Kunz and White, 2019 and references therein).

Graphitic metapelites are the main lithotype of the Kinzigite Formation and evolve from mica schists to migmatites with increasing metamorphic grade (Fig. 1; Redler et al., 2012, 2013). *P–T* conditions obtained by forward modelling indicate conditions from 0.4 to 0.8 GPa and 640–710 °C in the amphibolite facies and 0.8–1.2 GPa and 820–950 °C at granulite facies (Redler et al., 2012). Additional constraints from Zr-in rutile in the metapelites indicate peak metamorphic conditions up to UHT conditions >900 °C (Ewing et al., 2013; Luvizotto

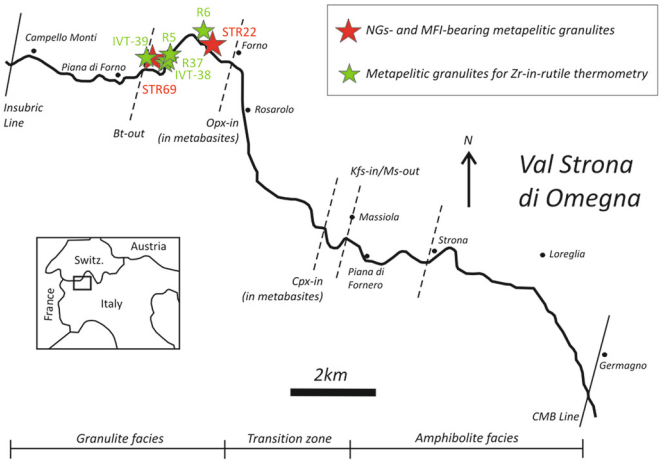

Fig. 1. Schematic map of Val Strona di Omegna (redrawn from Redler et al., 2012), with the position of the extrapolated mineral isograds and the samples considered in this work. NGs- and MFI-bearing granulites are from Carvalho et al. (2019), whereas granulites for Zr-in-rutile thermometry are from Luvizotto and Zack (2009) and Ewing et al. (2013).

and Zack, 2009).

In the study of Carvalho et al. (2019), NGs were investigated in graphitic metapelites from Val Strona di Omegna, throughout the IVZ sequence. Target rocks were the residual, melanocratic domains of garnet-bearing metatexites from middle amphibolite facies and transition zones, and in diatexites from the granulite facies zone. For all studied samples NGs and MFI coexist in the same clusters in the garnet, consequently they were interpreted as evidence for the immiscibility of melt and a C–O–H fluid at conditions high above the solidus. Since constraining the existence of prograde C–O–H fluids during HT to UHT metamorphism is of paramount importance for evaluating models on carbon cycling, here we focus specifically on IVZ graphitic granulites (Fig. 1). The reader interested to know more about NGs and MFI in amphibolite-facies rocks may refer to Carvalho et al. (2019) and Bartoli and Carvalho (2021).

4. Methods

Back-scattered electron imaging (BSE) were carried out with a CAMSCAN MX2500, equipped with LaB6 cathode, at the Dipartimento di Geoscienze, University of Padova.

Micro-Raman measurements of MFI in garnet were performed on polished thick sections at the Faculty of Science Research and Instrument Core Facility of Eötvös University (ELTE FS-RICF), Hungary, using a HORIBA LabRam HR Raman microspectrometer, with a frequency-doubled Nd:YAG laser with 532 nm excitation wavelength. A petrographic microscope Olympus (100× objective) was used to focus the laser on the selected inclusions. Raman spectra in the ranges 100–1800 cm^{-1} and 2700–3800 cm^{-1} were collected with an integration time of 10–15 s, and three accumulations. Raman maps of the inclusions were also performed on preserved inclusions below the host surface. Spectra in this case were acquired using a 100 μm confocal hole, 600 grooves/mm optical gratings, 2–3× accumulations and 12 s acquisition time. Measurements of fluid inclusions in experimental runs were conducted at the Dipartimento di Geoscienze, (Università di Padova, Italy), using a WITec confocal Raman alpha 300 R. Spectra were obtained using a 100 μm confocal hole, 300 or 1800 grooves/mm optical gratings, 4× accumulations and 15 s acquisition time. All data were processed using *LabSpec v5.41.15* and the solid phases inside the inclusions were identified using the data from the literature (Frezzotti et al., 2012b).

Inclusions previously mapped by Raman and located up to 10 μm below the garnet surface, were further investigated by serial sectioning using a FEI QUANTA 3D focused ion beam-scanning electron microscope (FIB-SEM) at ELTE FS-RICF, Hungary. The analyses were conducted using a 15 kV accelerating voltage and 23.7–190 pA current. The selected area was covered by a thin platinum layer (ca. 2 μm) in order to make the sample surface more resistant to mechanical abrasion of the Ga^{+} ion beam. At an initial stage, a high current Ga^{+} is used to make three trenches around the selected inclusion, and afterwards a low current ion beam was used to slice 280 nm-thick foils and gradually expose the target inclusion. Imaging of the exposed surface was acquired under BSE and SE, additional EDS of the solid phases were also obtained.

Experimental runs using a single-stage, end-loaded piston cylinder apparatus at the Laboratory of Experimental Petrology, Dipartimento di Scienze della Terra, (Università di Milano, Italy) were performed to re-homogenize nanogranitoid inclusions in garnet under the following conditions (additional information in Carvalho et al., 2019): 850 °C – 1 GPa, 20 h (sample IVT21) and 900 °C – 1.2 GPa, 5 h (sample STR22). In this study, the fluid inclusions coexisting with well re-homogenized melt inclusions in garnet have been investigated in these experiments to evaluate their behavior before down-temperature fluid-host interaction (see details below).

Phase equilibria modelling was performed using Perple_X software, version 6.9.1 (Connolly, 2009), to better constrain i) garnet and rutile formation and ii) chemistry of crustal melts. In the first case (i), calculations were done in the ten component MnO–Na_2O–CaO–K_2O–FeO–MgO–Al_2O_3–SiO_2–H_2O–TiO_2 (MnNCKFMASHT) system. Two bulk rock compositions were selected for this part, in particular, the average shale of Ague (1991), and an amphibolite-facies metapelite from the IVZ (IZ061, Redler et al., 2012). To facilitate the comparison, two *P–T* pseudosections were calculated for each bulk rock composition, using datasets ds62 (Holland and Powell, 2011) and ds55 (Holland and Powell, 1998, as revised in 2003), respectively. The following *a–x* relations were selected (dataset ds62): melt, garnet, orthopyroxene, muscovite, biotite and cordierite from White et al. (2014a, 2014b), ilmenite from White et al. (2000), plagioclase and K-feldspar from Holland and Powell (2003). For ds55, the *a–x* relations were: melt from (White et al., 2007), garnet from Holland and Powell (1998), biotite from Tajčmanová et al. (2009), white mica from Coggon and Holland (2002), plagioclase from Newton et al. (1980a) and K-feldspar from Thompson and Hovis (1979); an ideal model was used for cordierite and ilmenite. Fe_2O_3 was not considered to allow the comparison between old and new *a–x* models. A preliminary test on IVZ metapelite (considering dataset ds62) demonstrated that the lower pressure limit for the stability of rutile appears to be lower of about 0.1 GPa when Fe_2O_3 is excluded, without affecting the temperature effect of rutile formation (not shown). In the second case (ii), calculations were undertaken in the MnO–Na_2O–CaO–K_2O–FeO–MgO–Al_2O_3–SiO_2–H_2O–TiO_2–O (MnNCKFMASHTO) chemical system. The bulk rock composition selected for this part is the shale (Ague, 1991) originally modeled by Nicoli et al. (2022) with the software rhyolite-MELTS. In this way, it is possible to compare melt compositions modeled by Perple_X and rhyolite-MELTS. Datasets ds62 (Holland and Powell, 2011) and the available *a–x* models were used (listed above). Three different H_2O contents were alternatively considered (1, 2 and 3 wt%). Melt compositions were calculated along a prograde path from 700 °C and 0.5 GPa to 900 °C and 1.15 GPa, followed by an isothermal decompression path to 0.7 GPa, as done in Nicoli et al. (2022). Calculations were performed assuming both closed and open systems. In the latter case, two melt loss events were simulated along the P-T path. The volumes of melt extracted in each step and, in turn, the temperatures of each melt loss event, vary in function of the initial bulk H_2O content (i.e., rock productivity): 7 and 7 wt% melt at 800 and 875 °C for 1 wt% H_2O, 10 and 18 wt% melt at 750 and 850 °C for 2 wt% H_2O, 20 and 20 wt% melt at 750 and 850 °C for 3 wt% H_2O. Increasing the number of melt-loss events, diminishing contemporaneously the amount of melt drained at each step does not change the overall topology of phase diagrams (Bartoli, 2017). After each melt loss event, a new phase diagram was calculated with the modified bulk composition. It is important to note that the melt models available for phase equilibria modelling in high-grade metamorphic rocks do not account for the solubility of carbonic species and, therefore, cannot be used to quantify carbon mobility during anatexis. All the bulk rock compositions used in these calculations and those of modeled melts are reported in Supplementary Tables S1 and S2 (respectively), along with the calculated P–T pseudosections for bulk composition with 3 wt% added H_2O considering open and closed systems (supplementary Fig. S1).

5. Results

5.1. Petrographic features of graphite-bearing metapelitic granulites

Granulite facies metapelites from IVZ contain abundant garnet, prismatic sillimanite and rutile along with quartz, K-feldspar, graphite and minor plagioclase, whereas prograde biotite is absent or rare. In the older literature, these rocks are called “stronalites” (Schmid, 1968). Main accessory minerals in these rocks are zircon, monazite, apatite and rutile (Bea and Montero, 1999). Graphite is a common accessory phase in metapelites from this sequence, and although its amount decreases with increasing metamorphic grade, this mineral is still present in granulite-facies samples. Typically, graphite can be found in the matrix (Fig. 2a) and as inclusions in garnet.

Garnet may contain abundant inclusions (Fig. 2b–d) as isolated clusters or forming zonal arrangements suggesting a primary

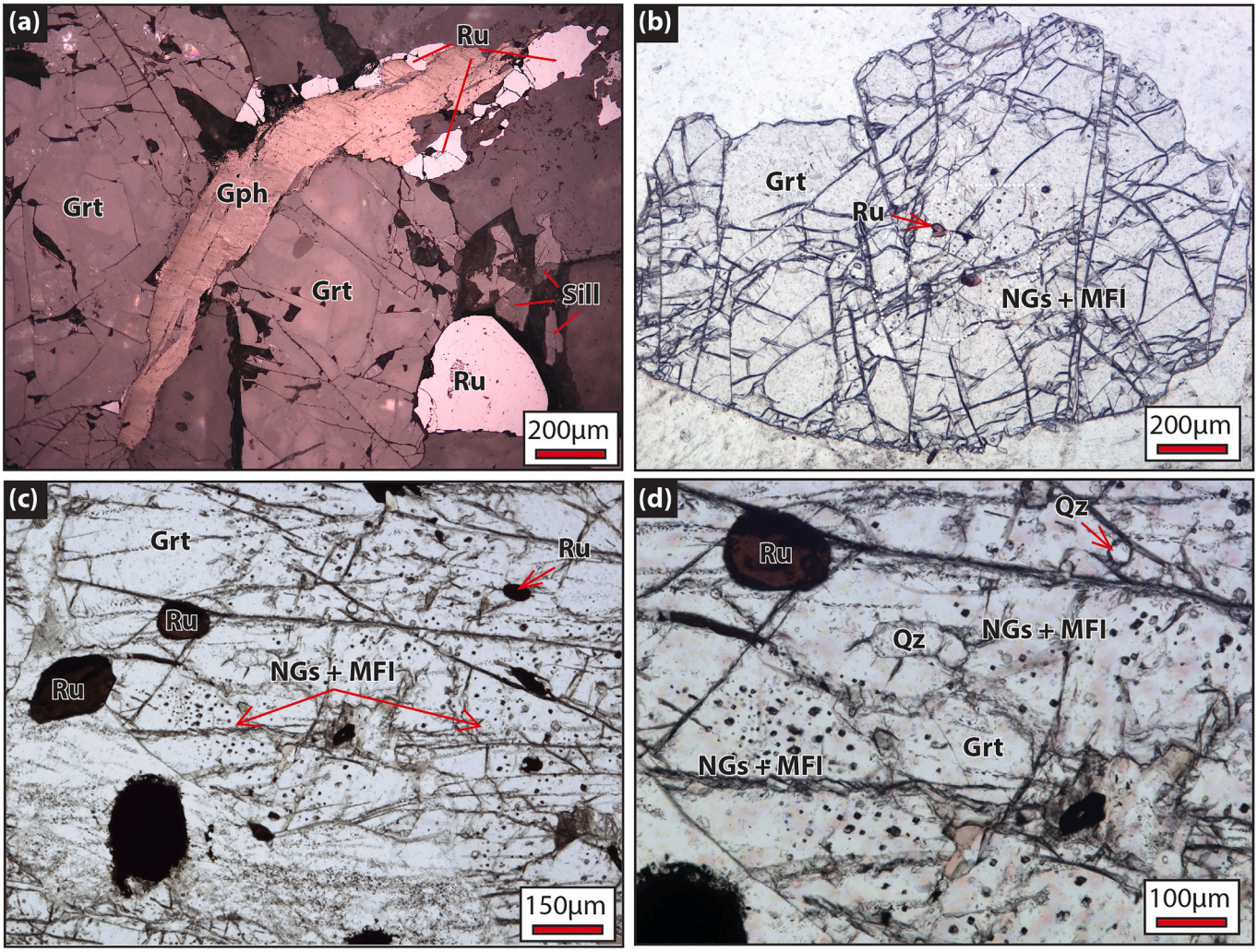

Fig. 2. Microstructural aspects of graphite-bearing granulites of Ivrea-Verbano Zone. (a) Large graphite flake associated to garnet, rutile and sillimanite (under reflected light). (b), (c) and (d) Microstructural evidence for the coexistence of rutile with NGs and MFI inside garnet from a IVZ metapelitic granulite (under plane polarized light). (d) is a close up of the image in (c). Grt = garnet; Gph = graphite; Sill = sillimanite; Ru = rutile; Qz = quartz; NGs = nanogranitoids; MFI = multiphase fluid inclusions.

entrapment. Carvalho et al. (2019) identified former melt and fluid inclusions. Melt inclusions (i.e. NGs) are crystallized into a granitic phase assemblage of quartz, plagioclase, K-feldspar and biotite (Fig. 3a). Graphite is a common accidentally trapped phase in NGs (see Fig. 4 in Carvalho et al., 2019), as it usually occurs partially enclosed in the host garnet and may still be present after re-homogenization experiments. Some inclusions may also contain rutile as a trapped mineral (Fig. 3a).

Fluid inclusions (i.e. MFI) are characterized by the presence of a C–O–H–N residual fluid (see details below) together with siderite, calcite, pyrophyllite and kaolinite (Figs. 3b, 4a–i and 5a), and in some cases rutile (Figs. 3b and 4b). In MFI, graphite can be either an accidentally trapped (Fig. 4a–b) or even a daughter phase (i.e. precipitated directly from the fluid); in the latter case, graphite appears as very small flake-like crystals located entirely within the inclusion volume, of which they occupy only 1–2%.

Mixed (fluid + melt) inclusions containing variable proportions of granitic mineral assemblage and carbonates, as well as variable volumes of voids, have also been reported in the same clusters of NGs and MFI (see Fig. 4e, f in Carvalho et al., 2019). Fig. 5b shows one of these inclusions, where serial sectioning during FIB-SEM analysis revealed the coexistence of K-feldspar, quartz and plagioclase together with siderite and calcite and a large porosity.

Rutile is found not only in the matrix of the rocks (Fig. 2a), but also as mineral inclusions in garnet closely associated with NGs + MFI clusters (Fig. 2b–c) and as an accidentally trapped mineral (i.e. rutile has not crystallized from the melt or fluid) within single NGs (Fig. 3a) and MFI (Figs. 3b and 4b). These observations demonstrate the coexistence of melt and C–O–H fluid (i.e. fluid-melt immiscibility) in the rutile stability field of IVZ metapelitic granulites (see details below).

5.2. *Fluid composition at granulite facies conditions*

Micro-Raman spectroscopy measurements of unexposed inclusions before re-homogenization experiments indicate that the solids within MFI are mainly carbonates + pyrophyllite ± kaolinite ± graphite ± rutile, whereas the residual fluid phase contains variable proportions of CO_2, CH_4 and N_2 (Fig. 4e–g). Carvalho et al. (2019, 2020) showed that different proportions of fluid species may be present in different inclusions coexisting in the same sample, as well as different solid-porosity ratios. Specifically, solids make up to 67%, whereas the porosity filled up by the residual fluid varies from 33 to 48%, which can be either rich in CO_2 or in CH_4. H_2O and other fluid species were not detected in the residual fluid. Using the method from Dubessy et al. (1989), the relative proportion of fluid species in the residual fluid varies in the ranges 0–86 mol% CO_2, 18–23 mol% N_2 and 0–76 mol% CH_4. In these MFI, CO_2 density, calculated using the method from Wang et al. (2011), varies

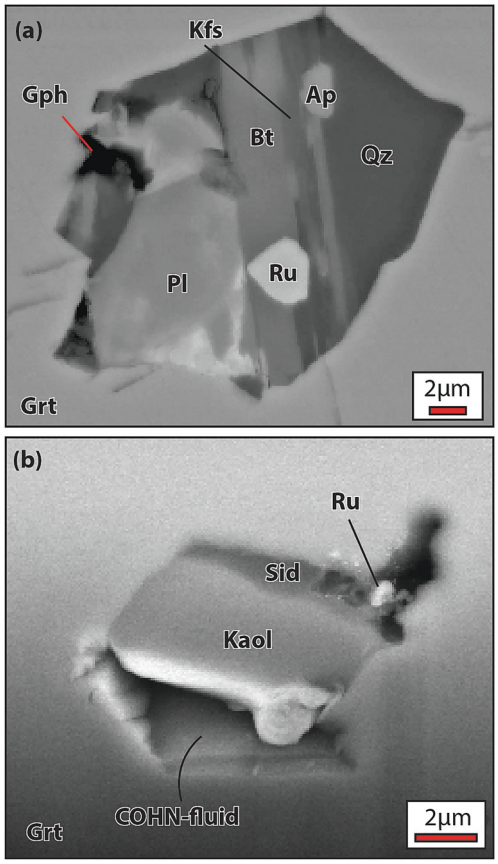

Fig. 3. (a) BSE image of a nanogranitoid from a IVZ metapelitic granulite (modified after Carvalho et al., 2020) containing plagioclase (Pl), K-feldspar (Kfs), quartz (Qz), biotite (Bt). Apatite (Ap) and graphite (Gph) are also present and represent accidentally trapped minerals. (b) BSE image of a MFI from a IVZ metapelitic granulite exposed during FIB-SEM analyses (see Raman map of this inclusion in Fig. 4b). It contains accidentally trapped rutile, graphite and step-daughters minerals siderite (Sid), pyrophyllite (Prl) and kaolinite (Kaol).

from 0.1 to 0.7 g/cm^3 (0.4 ± 0.2 in average) (Fig. 6a, c).

After high-T re-homogenization, fluid inclusions can be quite dark (Fig. 4j) and micro-Raman measurements (Fig. 4j–m) show the presence of graphite and a fluid component that is mostly composed of CO_2 and CH_4, and sometimes with N_2. A CO component has been rarely observed. Like in MFI before rehomogenization, H_2O or other fluid species were not detected in the fluid phase. The relative proportions of fluid species (calculated with the method by Dubessy et al., 1989) varies from 71 to 96 mol% CO_2, 3.6–28 mol% CH_4 and 0–13.7 mol% N_2 in the fluid inclusions in experiment performed at 850 °C, and from 30 to 86 mol% CO_2, 14.2–70 mol% CH_4 and 0–3.5 mol% CO in the experiment performed at 900 °C. Graphite within the inclusions commonly has low crystallinity, as demonstrated by the presence of both high intensity peaks at 1581 and 1353 (Fig. 4m). Carbonate, that was found in all the natural MFI (>100 inclusions), has been observed only in three out of 30 inclusions after experiments. The density of CO_2 in re-homogenized inclusions is in most cases considerably higher than what has been measured in natural MFI (see Fig. 6b–c for a comparison). The highest value is 1.06 g/cm^3 (Fig. 6b) and the average is 0.6 ± 0.3 g/cm^3.

5.3. Thermal constraints from garnet and rutile

Thermodynamic modelling shows that both investigated metapelite bulk rocks display the classic prograde sequence of melting reactions experienced by natural metapelites: production of melt at the wet solidus, dehydration-melting of muscovite forming K-feldspar, and incongruent breakdown of biotite producing ferromagnesian minerals. In particular, Figs. 7 and 8 show the modeled amounts of garnet, rutile and biotite for the two bulk rocks, comparing computational outputs of datasets ds62 and ds55, respectively (see Methods). Considering dataset ds62, the re-parameterized *a–x* models and the field gradient proposed for IVZ, garnet and rutile should form up to 830–840 °C, representing also the maximum temperatures for the stability of biotite (Figs. 7a–c and 8a–c). Above these temperatures, garnet and rutile are still present, but they are not expected to increase their modal amount. In contrast, for calculations considering dataset ds55, about 40 to 50% of garnet is predicted to form between 850 and 900 °C (Figs. 7d and 8d). Similarly, rutile mostly or totally grows in this temperature range, and biotite can be stable up to 900 °C (Figs. 7e–f and 8e–f).

Rutile from most IVZ metapelites is texturally constrained to have grown in equilibrium with quartz and zircon and it has been object of a number of studies focused on the application of Zr-in-rutile thermometer (e.g., Luvizotto and Zack, 2009; Ewing et al., 2013; Pape et al., 2016). Taking advantage of the great amount of rutile data available for rocks from Val Strona di Omegna, here we compiled 107 analyses done in granulites (Luvizotto and Zack, 2009; Ewing et al., 2013) sampled close to outcrops where NGs from Carvalho et al. (2019) were collected (Fig. 1). Applying the equation recently refined by Kohn (2020) for Zr-in-rutile thermometer and selecting the values above the ninetieth percentile to delete effects of diffusional resetting (Luvizotto and Zack, 2009), the calculated temperatures for IVZ granulite-facies rocks intersect the rutile stability field at >890 °C for rutile included in garnet and at >900 °C for grains in the matrix (Figs. 7b and 8b). Ewing et al. (2013) estimated that the analytical uncertainties alone should result in an error of ±15–25 °C on Zr-in-rutile temperatures, whereas the uncertainty inherent in Kohn's (2020) calibration is ±15 °C.

5.4. Natural versus modeled melts by Perple_X and rhyolite-MELTS

P–T pseudosections are presented in Supplementary Fig. S1, whereas model melts by Perple_X (this study), by rhyolite-MELTS (Nicoli et al., 2022) and the natural melt compositions from IVZ (Carvalho et al., 2019) are compared in Figs. 9 and 10. Melt compositions were calculated along the *P–T* path proposed by Nicoli et al. (2022) (see Fig. 7a).

Results shows that in terms of ASI [molar $Al_2O_3/(CaO + Na_2O + K_2O)$] and AI [molar $Al_2O_3 - (Na_2O + K_2O)$] Perple_X predicts melt compositions which are much more consistent with those of IVZ NGs (see Fig. 9a–c). In contrast, the results from rhyolite-MELTS (presented by Nicoli et al., 2022) fail to reproduce ASI and AI of the natural melt compositions (Fig. 9a). Albeit not as clearly seen as in Fig. 9a, a better match is observed for natural melts and the melts modeled with Perple_X also when considering other chemical parameters such as molar Ca/(Ca + Na), SiO_2 and #Mg. This is clearly displayed by the arrows representing Perple_X which plot mostly inside the pink dashed box and by the fact that rhyolite-MELTS arrows plot mostly outside the average of NGs (Fig. 9d–g; see further discussion below).

Concerning H_2O, the contents predicted by rhyolite-MELTS are not reported by Nicoli et al. (2022), but they can be visually estimated from their Fig. 2a: H_2O decreases from about 12.5 to about 2.5 wt% along the prograde path from upper amphibolite to granulite-facies conditions. Conversely, Perple_X predicts a narrower range (3.4 to 9.2 wt%; see Supplementary Table S2) that overlaps much better with the H_2O contents measured by nanoSIMS in the NGs (Fig. 10). As Perple_X cannot model CO_2 contents of melt, this parameter cannot be compared.

6. Discussion

6.1. Composition of C–O–H fluids in graphitic granulites

The two types of polycrystalline inclusions in the graphitic granulites from IVZ have been studied in past works (Carvalho et al., 2019, 2020)

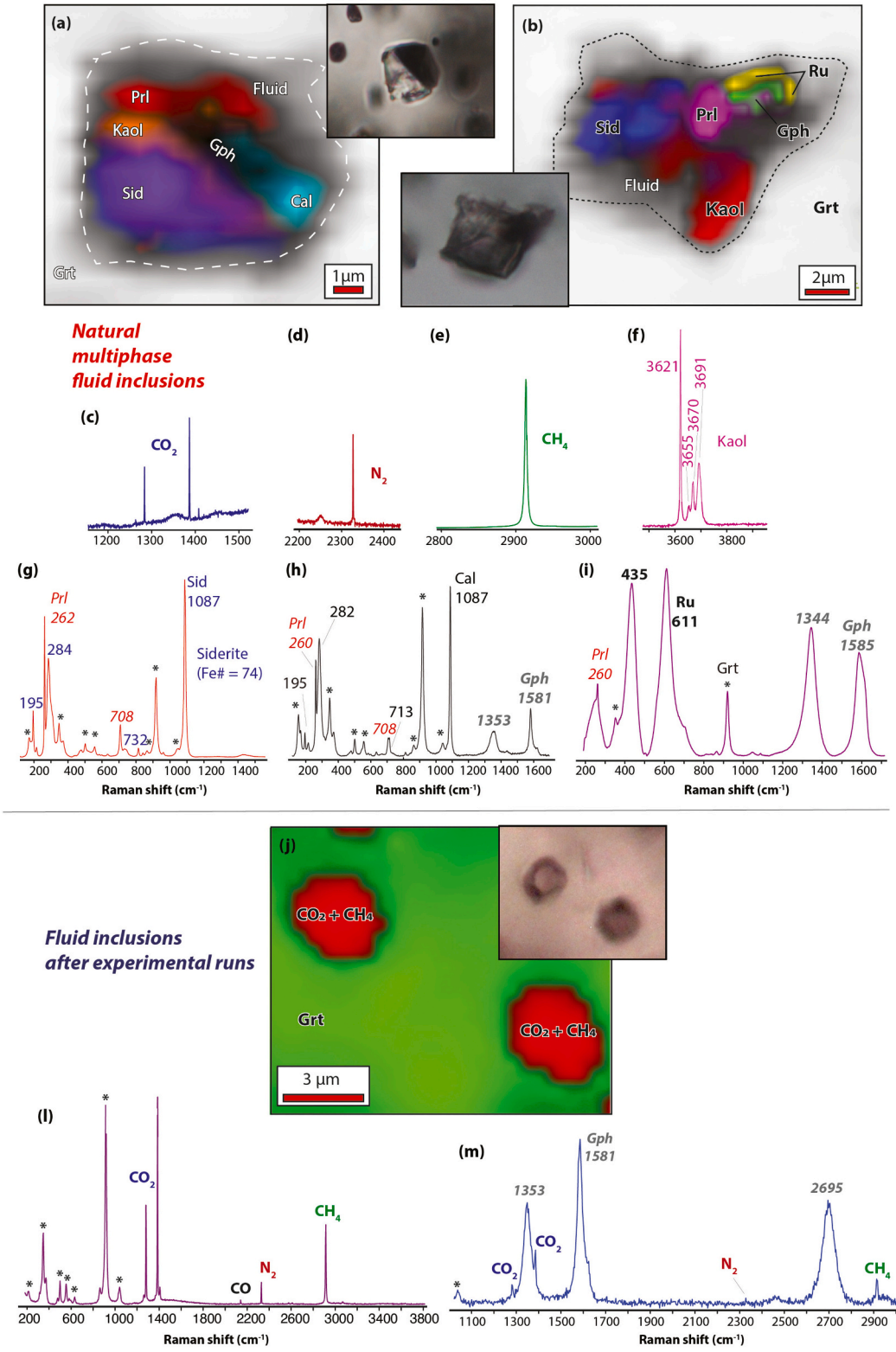

Fig. 4. (a) and (b) Raman maps, inset photomicrographs and (c)-(i) Raman spectra of MFI from IVZ metapelitic granulite. (j) Raman map and photomicrograph of fluid inclusions after experimental runs. Red area represents the overlapping position of CO_2 and CH_4 within the inclusions. (l)-(m) Raman spectra of the fluid inclusions after experimental runs. Characteristic peaks of garnet (Grt) are represented as *. Abbreviations: Sid = siderite; Prl = pyrophyllite; Cal = calcite; Kaol = kaolinite; Ru = rutile; Gph = graphite. Raman map in (a) is modified after Carvalho et al. (2020) with the permission from Elsevier. This article was published in Earth and Planetary Science Letters, vol. 536, Carvalho et al., Primary CO_2-bearing fluid inclusions in granulitic garnet usually do not survive, 116,170, Copyright Elsevier (2020). (For interpretation of the references to colour in this figure legend, the reader is referred to the web version of this article.)

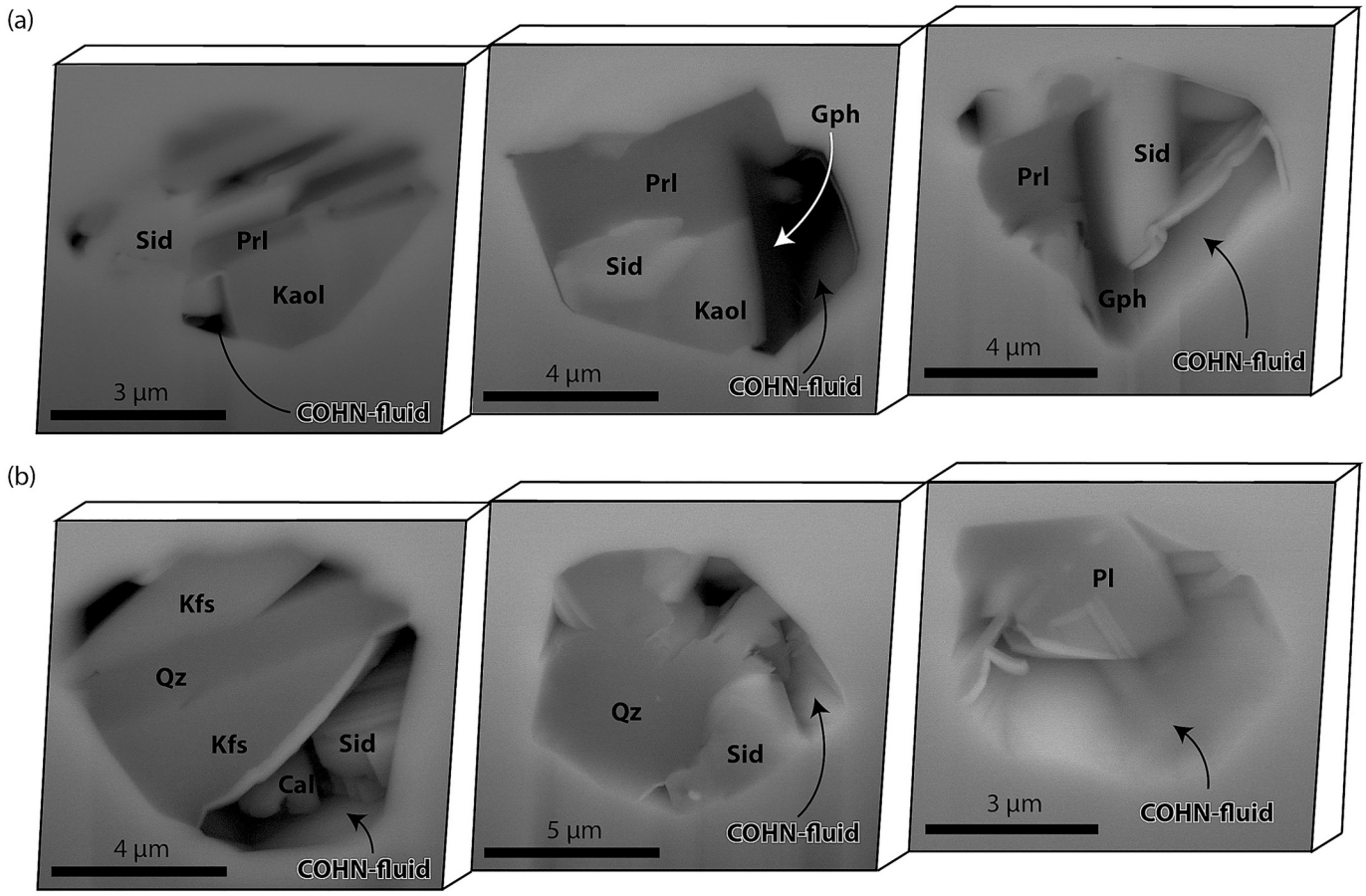

Fig. 5. FIB-SEM slices of (a) MFI and (b) mixed melt-fluid inclusion. Abbreviations as in Figs. 3 and 4.

which interpreted that the phase assemblage observed at ambient conditions within NGs and MFI represents the product of processes occurring during cooling – i.e. melt crystallization in NGs (Cesare et al., 2009, 2015) and fluid-garnet interaction in MFI (e.g., Tacchetto et al., 2019).

Coexistence of primary melt and fluid inclusions in the same clusters in garnet indicates that melt and fluid were immiscible in the studied graphitic granulites at the time of garnet growth. This interpretation is further confirmed by the presence of mixed (melt + fluid) inclusions containing variable proportions of the two phase and displaying variable porosity. These inclusions indicate that heterogenous entrapment (Roedder, 1984) took place, and as a result, intermediate compositions between the melt and fluid end-members were recorded. Mixed inclusions have been reported also in other case studies of fluid-melt immiscibility in migmatites and granulites (e.g. Cesare et al., 2007; Ferrero et al., 2014; Gianola et al., 2021).

Evaluating the precise composition of the fluids that was originally present in the MFI is hampered by their partial consumption in the formation of stepdaughter phases. Micro-Raman and FIB-SEM investigations allow to constrain the fluid as a C–O–H–N mixture of H_2O, CO_2, CH_4 and N_2. Concerning the behavior of graphite, the detection of both CH_4 and CO_2 in the residual fluid of MFI indicates that the C–O–H–N fluid trapped at high temperature in the inclusions had the potential to precipitate some daughter graphite by respeciation upon cooling (Cesare, 1995), so that the ambient T fluid would be less carbonic than the primary one.

A better quantification of the fractions of each species would require estimating the volume and density of the residual fluid, as well as the volumes of each stepdaughter carbonate and hydroxylated phase, as discussed by Carvalho et al. (2020). They used a FIB-SEM-based 3D reconstruction of four MFI in IVZ to back calculate the composition of the fluid before the interaction with the garnet. The estimated composition of the fluid, assumed as a binary H_2O–CO_2 mixture, had an X_{CO2} in the range 0.55–0.70.

The above estimates on fluid composition may suffer from drawbacks such as i) the large errors in the 3D volume reconstruction, ii) the uncertainties in the volatile contents of the micron-sized stepdaughter crystals, especially the hydroxylated phases pyrophyllite and kaolinite, iii) the distinction between trapped and stepdaughter graphite and, not least iv) the very time-consuming and expensive nature of the characterization by FIB-SEM serial sectioning.

An alternative way to quantify the original composition of fluids in MFI could be the reconstitution of the fluid after MFI re-homogenization. In this work, we have succeeded in analyzing some re-homogenized MFI from the remelting experiments at 850° and 900 °C. Most of them do not contain any longer solid phases, except for rare carbonate and coatings of poorly crystalline graphite at inclusion walls. The fluid species detected in these inclusions are CO_2, CH_4 and N_2, and the density of CO_2, up to 1.06 gcm^{-3}, is greater than in the natural MFI. These features confirm the C–O–H–N nature of the fluid and are in agreement with the reversion of the process of interaction between such fluid and the host garnet that formed the stepdaughter crystals in the MFI. However, the presence of the H_2O component, required for the formation of pyrophyllite and kaolinite and predicted by the simultaneous occurrence of CO_2 and CH_4 in the inclusions (Cesare, 1995), has not been detected. It is well known that H_2O can be easily overlooked as it may occur as thin films (<0.1 µm) on the inclusion walls (e.g., Berkesi et al., 2009; Lamadrid et al., 2014). Another possibility is leakage of H_2O from the inclusions through diffusion (e.g. Bakker and Jansen, 1991;

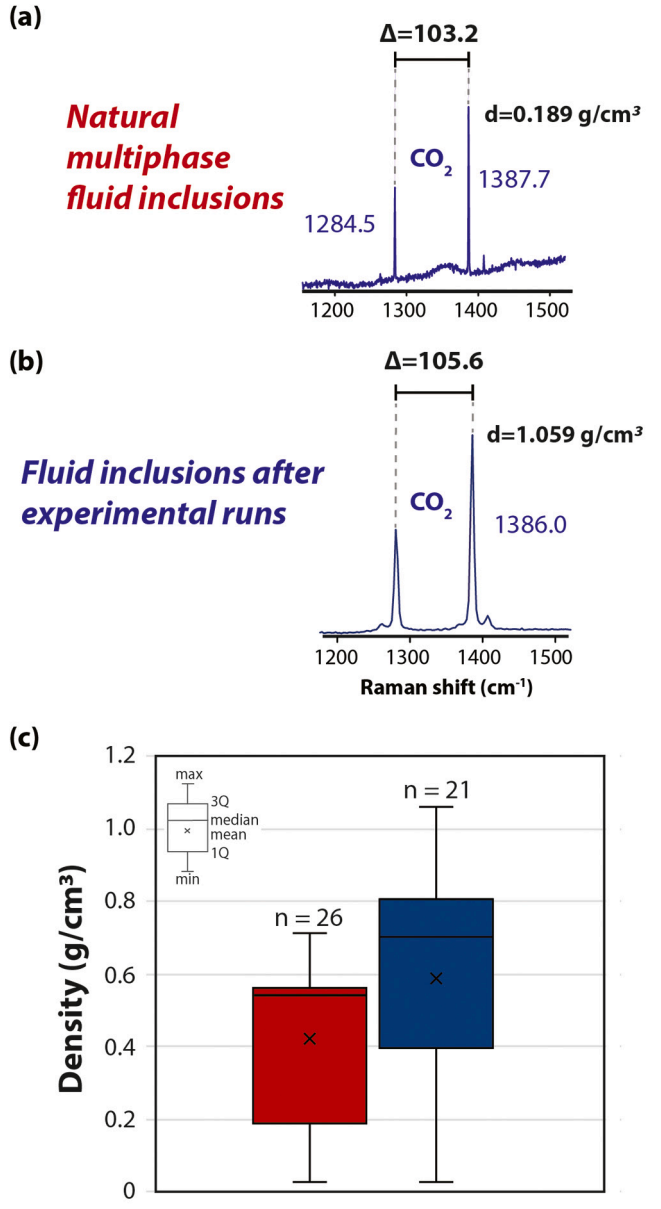

Fig. 6. (a) and (b) Raman spectra of CO_2, Fermi doublet (Δ) and calculated density of natural and experimentally-treated fluid inclusions, respectively. (c) Whisker plot diagram of density (g/cm^3) of natural (left, red) and experimentally-treated fluid inclusions (right, blue). (For interpretation of the references to colour in this figure legend, the reader is referred to the web version of this article.)

Frezzotti et al., 2012a). In particular, H_2O loss has been identified as an important post-entrapment process in other case studies of multiphase fluid inclusions (Maffeis et al., 2021; Spránitz et al., 2022). Regardless of the actual cause for the lack of detection of H_2O, it is apparent that this is a major problem in the quantification of the composition of the C–O–H–N fluid originally in equilibrium with the granitic melt at granulite facies, and it requires further studies.

The data presented here may suggest that multiphase fluid inclusions have been (at least to some degree) re-homogenized with the piston cylinder, at present this approach is experimentally challenging and results are not yet satisfactory. A better strategy is to investigate the potentials of other techniques (e.g. hydrothermal diamond anvil cell; Li et al., 2017) that allow homogenization of the inclusions to be monitored optically during heating.

6.2. Fluids and melt inclusions in granulitic garnet

The presence of NGs and/or MFI in UHT graphitic granulites does not automatically imply that they represent HT to UHT melts and fluids. Their occurrence within peritectic garnet in the graphitic granulites from IVZ implies solely that they were trapped during prograde to peak conditions (i.e. during heating) as a consequence of incongruent melting reactions (Cesare et al., 2009). Phase equilibria modelling of anatectic metapelitic rocks generally predict that garnet should be growing upon the temperature interval between 750 and 850 °C, at pressures typical of orogenic metamorphism, via partial melting reaction consuming biotite (e.g., Johnson et al., 2021). This is also evident from garnet and biotite isomodes of Fig. 7a–c and 8a–c, constructed using the internally consistent thermodynamic dataset, ds62, of Holland and Powell (2011) and the pertaining *a–x* models (see Methods). Similarly, rutile shows prograde growth in the temperature window 750–850 °C (Figs. 7b, 8b), associated with the breakdown of Ti-bearing biotite. However, these predicted temperatures do not match those provided by Zr-in-rutile thermometer (> 890 °C).

Being the main sink for Fe, Mg and Ti among reactants during incongruent melting reactions, biotite behavior impacts on the modal proportion of garnet and rutile. Recently, Gervais and Trapy (2021) have tested different sets of a–x models against partial melting experiments of metasedimentary rocks and have found that the biotite model of Tajčmanová et al. (2009) yields better results when compared to the experiments. Using this model, as well as the dataset ds55, the biotite-out curve for the investigated metapelites shifts towards higher temperatures with respect to dataset ds62 (from 830° to 870–900 °C) (Figs. 7c,f and 8c,f). As a consequence, garnet and rutile are predicted to grow up to 910 °C (Figs. 7d,e and 8d,e). In particular, ca. 50% of the garnet is expected to form between 850 and 910 °C in the metapelite IZ061 from IVZ (Fig. 8d).

Therefore, the use of the biotite model of Tajčmanová et al. (2009) reduces the gap between the predicted temperatures for garnet and rutile formation, and the temperatures provided by Zr-in-rutile thermometer (Figs. 7 and 8). It is worth noting that fluorine currently cannot be modeled as a component in phase equilibria calculations, despite its effect in enhancing the biotite stability to higher temperatures (e.g., Peterson et al., 1991). Biotite from metapelites of Val Strona di Omegna shows F content ranging from 0.60 (transition zone) to 2.10 wt% (granulite-facies; Harlov and Förster, 2002). The latter values are higher than F contents of biotite from melting experiments of metapelites where biotite survived up to ≈975 °C (at 1 GPa; Patiño Douce and Johnston, 1991). Therefore, we cannot exclude that biotite stability exceeded 900 °C in IVZ granulites and, as a consequence, that garnet and rutile grew at UHT conditions.

To sum up, in the case study of IVZ granulites, the coupling of microstructures (Figs. 2 and 3), Raman data of MFI (Fig. 4), phase equilibria modelling and Zr-in-rutile thermometry (Figs. 7 and 8) clearly supports the coexistence of anatectic melt and a C–O–H fluid at least near UHT conditions. Notably, such conditions are significantly higher than the 700–750 °C proposed by Nicoli et al. (2022) for IVZ crustal section.

6.3. Possible causes for the mismatch between models and nature

To quantify the flux of carbon related to the burial of siliciclastic sediments in the lower crust, Nicoli et al. (2022) simulated partial melting of (meta)sediments (shale and greywacke), comparing model predictions in terms of melt compositions, including H_2O and CO_2 contents, with those measured in NGs. Their failure to predict the occurrence of C–O–H fluid-melt immiscibility up to near UHT in the IVZ metapelites probably resides in the choice of the thermodynamic software rhyolite-MELTS to reproduce melting equilibria of

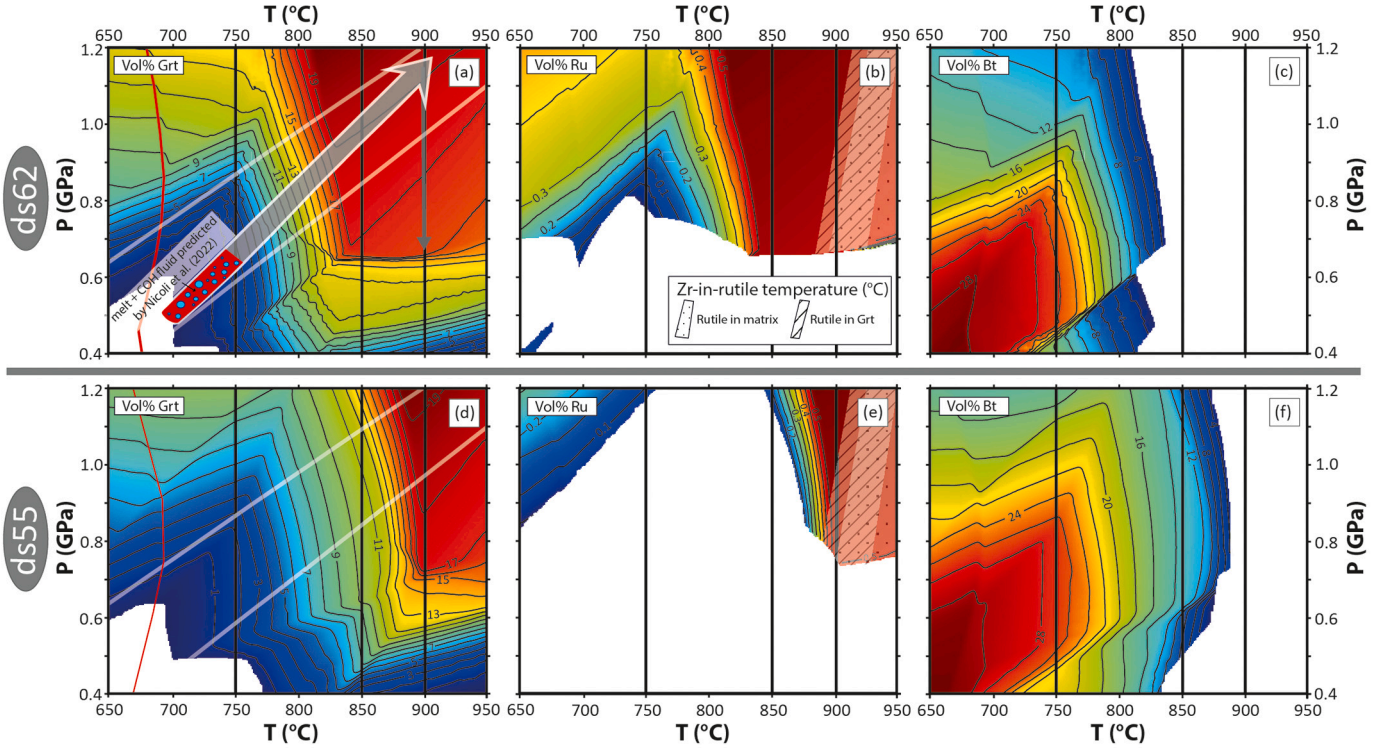

Fig. 7. Comparison between mode isopleths of garnet, rutile and biotite, based on P–T pseudosections derived from the two datasets ds62 and ds55 and calculated for the average shale composition (Ague, 1991). Red curve: solidus. The two white lines delimit the metamorphic field gradient in Val Strona di Omegna (from Redler et al., 2012). Arrows in (a) represent the prograde and decompression paths along which melt compositions were calculated. The colored portion of the arrow reflects the extent of melt-fluid immiscibility proposed by Nicoli et al. (2022). Zr-in-rutile data are from Luvizotto and Zack (2009) and Ewing et al. (2013), and refer to IVZ metapelitic granulites. Only samples recording peak T are considered (i.e., samples without resetting). All these rocks come from Val Strona di Omegna, like those investigated by Carvalho et al. (2019, 2020). Zr-in-rutile temperatures were calculated using the calibration of Kohn (2020). (For interpretation of the references to colour in this figure legend, the reader is referred to the web version of this article.)

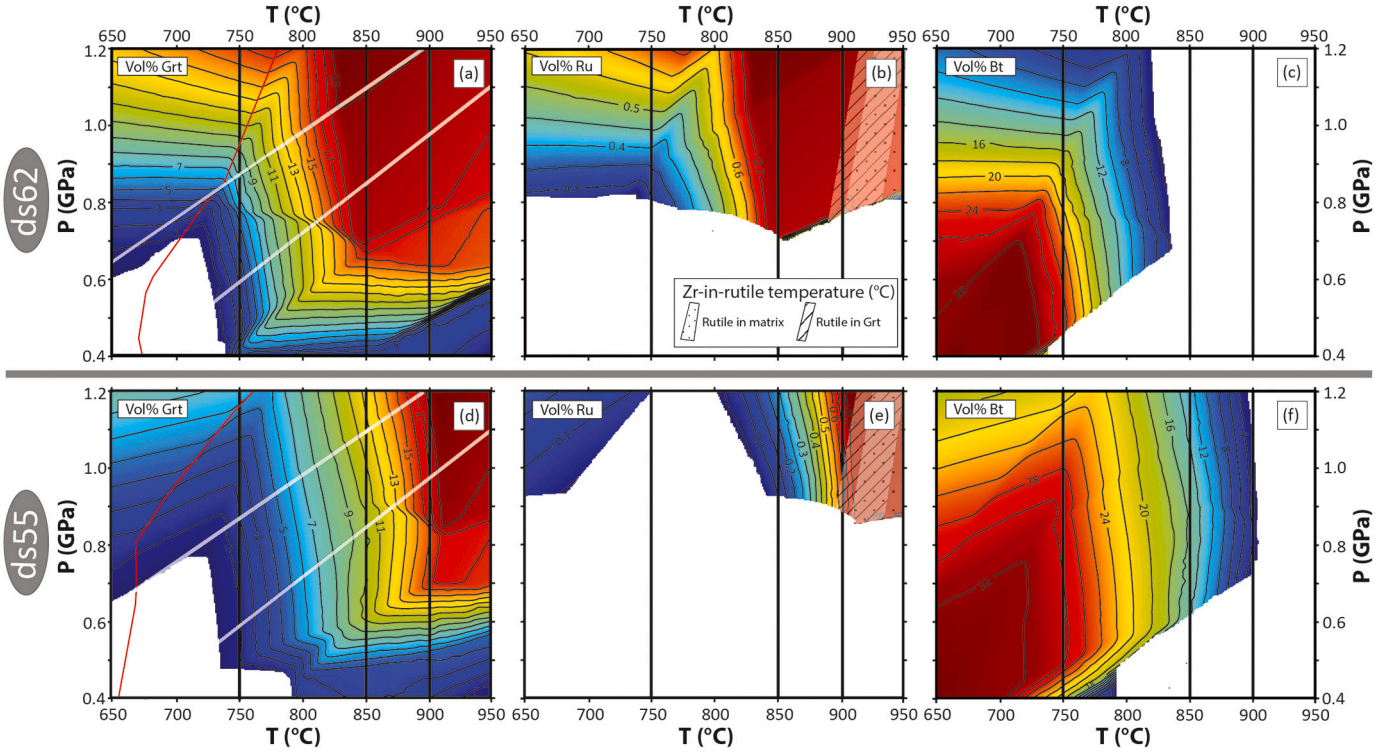

Fig. 8. Comparison between mode isopleths of garnet, rutile and biotite, based on P-T pseudosections derived from the two datasets ds62 and ds55 and calculated for an upper-amhibolite metapelite from IVZ (bulk composition IZ061 from Redler et al., 2012). Red curve, white lines and Zr-in-rutile data as in Fig. 7. (For interpretation of the references to colour in this figure legend, the reader is referred to the web version of this article.)

metasedimentary lithologies. In fact, as highlighted by the developers, rhyolite-MELTS is i) specifically designed "*to correctly predict the quartz + feldspar saturation surface in temperature, pressure and composition space*", ii) calibrated "*based on the well-constrained crystallization conditions of the early erupted Bishop Tuff magma*" and iii) considered "*very useful in constraining crystallization conditions*" (Gualda et al., 2012). Consequently, even if melting and crystallization behave similarly under the thermodynamic point of view, rhyolite-MELTS does not represent a conventional computational software to predict suprasolidus fluid-melt-rock equilibria during the prograde evolution of high-grade metamorphic rocks (Johnson et al., 2021). Indeed, Gardner et al. (2014) reported inconsistencies in the predicted stability of Fe-Ti oxides, pyroxene and biotite, and more recently, a similar observation was made for garnet, biotite and orthopyroxene (Zhang et al., 2021). Thus, the difficulty of rhyolite-MELTS in dealing with phase assemblage dominated by hydrous silicates (i.e., amphibole, biotite and muscovite; https://melts.ofm-research.org/) has important consequences for modelling crustal anatexis (Hernández-Uribe et al., 2022). Rather, concerning the migmatite realm, rhyolite-MELTS represents an extremely useful tool to simulate how feldspar-dominated fractional crystallization impacts the chemistry of melt-rich domains (e.g. metaluminous to weakly peraluminous leucosomes; Carvalho et al., 2016).

Additional complexity in applying rhyolite-MELTS to predict melting equilibria in metasedimentary rocks is related to software's difficulty to deal with strongly peraluminous melts (ASI > 1.1; i.e., those derived from metasediments), simply because it was not calibrated for these melt compositions (e.g. Yang et al., 2022). According to the results presented in Nicoli et al. (2022), rhyolite-MELTS predicts ASI values between 1.8 and 2.8 for IVZ melts (large arrows in Fig. 9), too high for pure anatectic melts derived from partial melting of metasedimentary rocks (Gao et al., 2016). The majority of IVZ NGs are instead characterized by much lower ASI (1.1–1.7) and AI (<0.09) as reported by Carvalho et al. (2019). It must be noted that Nicoli et al. (2022) reported ASI and AI values for IVZ melts which do not correspond to the real ones in the reference work of Carvalho et al. (2019) – compare Fig. 3a in Nicoli et al. (2022) and Fig. 8a in Carvalho et al. (2019), which theoretically should show the same data points. The incorrect ASI and AI values considered by Nicoli et al. (2022) for IVZ NGs are in the range 1.1–2.8 and 0.06–0.23, respectively. Similarly incorrect AI values are reported for NGs data from the Central Maine Terrane are considered – compare values in Fig. 3b in Nicoli et al. (2022) and Fig. 5c in Ferrero et al. (2021).

A comparison of model melt compositions obtained by Perple_X and rhyolite-MELTS and natural melts from IVZ shows that the former provides much better results, even if they are not perfect. In other words, due to limitations and pitfalls of each petrologic tool, including NGs (see the comparative study and discussion in Bartoli and Carvalho, 2021), some geochemical discrepancies between calculated and natural melts are also expected for Perple_X (Figs. 9 and 10). For example, natural melt compositions show a larger variability than the model melts, which can be likely related to the effect of local equilibrium volumes, different diffusivities of melt components, and/or the existing melt model (Bartoli et al., 2014; Acosta-Vigil et al., 2017; Bartoli and Carvalho, 2021). Nonetheless, Fig. 9 shows that the modelling of Nicoli et al. (2022) fails to reproduce the composition of IVZ melts and highlights the pitfalls which may be encountered when using a computational software for aims for which it was not developed nor calibrated.

6.4. Some problems with thermodynamic modelling of suprasolidus graphitic systems

Ghiorso and Gualda (2015) developed a H_2O–CO_2 mixed fluid thermodynamic model to be used with rhyolite-MELTS. This implementation was designed to examine H_2O and CO_2 partitioning between the melt and vapor phase accompanying crystallization along a specified temperature and pressure evolution path (Ghiorso and Gualda, 2015) and requires fixing an initial bulk composition, also in terms of H_2O and CO_2. Nicoli et al. (2022) used it to quantify the amount of mineral-bound bulk rock H_2O and CO_2 necessary to reproduce the volatile content of NGs, setting their runs for different H_2O and CO_2 contents in the starting sediments, assuming IVZ subsolidus metapelites as carbonate-rich siliciclastic metasedimentary rocks. However, these rocks are mostly graphitic metapelites with subordinate layers of metagreywackes, metabasites, and only minor calcsilicates and marbles (Quick et al., 2003). Therefore, carbon in regionally-metamorphosed subsolidus metapelites of IVZ is stored only in graphite, as demonstrated by petrographic observations (Carvalho et al., 2019).

From the obtained minimum amount of bulk rock CO_2 present at peak conditions, Nicoli et al. (2022) calculated a flux of carbon into the lower crust of 0.2–4.4 Mt. C/yr. These values are then converted to 0.18–3.8 Mt. C/yr lost to middle and upper crust by S-type granite magmatism, assuming that at least 88% of the anatectic melt derived from siliciclastic sediments leaves the lower crust before/at peak metamorphism. In their calculations they implicitly assume that all the bulk CO_2 enters the melt phase, and yet this is overstated as demonstrated by IVZ granulites where residual graphite, carbon-bearing NGs and carbonate-bearing MFI are still observed under the microscope. Thus, their calculated carbon fluxes of the lower crust may be incorrect. Moreover, the assumption of Nicoli et al. (2022) of carbonate-rich siliciclastic metasedimentary rocks as source region of IVZ melts would demand considering that melting equilibria of carbonate-bearing rocks (calcareous pelites to argillaceous marls) are very different from those of common pelites, also in terms of melt productivity and CO_2 contents (Groppo et al., 2021).

A major problem of modelling melt-rock-fluid interactions in graphitic metapelites is to account/deal with the additional thermodynamic and mass balance constraints imposed by graphite on C–O–H fluid speciation. Connolly and Cesare (1993) noted that in dehydration-dominated graphitic systems such as metapelitic environments, the $X_O = 1/3$ model provides a good working hypothesis for fluid composition, where the fluid compositional variable X_O is $n_O/(n_O + n_H)$ (Connolly, 1995). In a graphite buffered assemblage and under normal metamorphic/anatectic conditions an $X_O = 1/3$ fluid is composed of H_2O and equal amounts of CO_2 and CH_4. The latter carbonic components amount to about 4 to 8 mol% of the fluid in the P–T range of interest for the IVZ metapelites. The behavior of such ternary H_2O–CO_2–CH_4 fluid at suprasolidus conditions cannot be modeled by any current software due to the lack of adequate melt models. Regardless of the quantitative aspects, one major qualitative implication is that, owing to the non-trivial presence of a CH_4 component and at the same time to the negligible solubility of CH_4 in crustal melts (Mysen et al., 2009), complete fluid-melt miscibility cannot be reached even at UHT conditions. In other words, the presence of graphite implies that in the absence of redox processes (e.g., Cesare et al., 2005) the fraction of CH_4 is destined to increase in the fluid, with respect to that of H_2O and CO_2, and that a C–O–H fluid must be present at >900 °C. Indeed, CH_4 (as well as N_2) is present in the MFI of all IVZ metapelites (Fig. 4). Another major implication is that the quantities of graphitic carbon dissolved in anatectic melts may be largely overestimated when using the current incomplete thermodynamic models.

To our knowledge, the computational study by Chu and Ague (2013) represents an advance in terms of modelling strategy for graphite-bearing metapelitic anatectic systems. The main merit of their work consists in the development of a new model of CO_2 solubility in felsic melts that was used in a MATLAB code set, applying algorithms similar to THERMOCALC. However, the key critical issues reported above of not considering the presence and behavior of CH_4 in the fluid phase still remain, as demonstrated by their predictions of C–O–H fluid stability only at $T < 750$ °C.

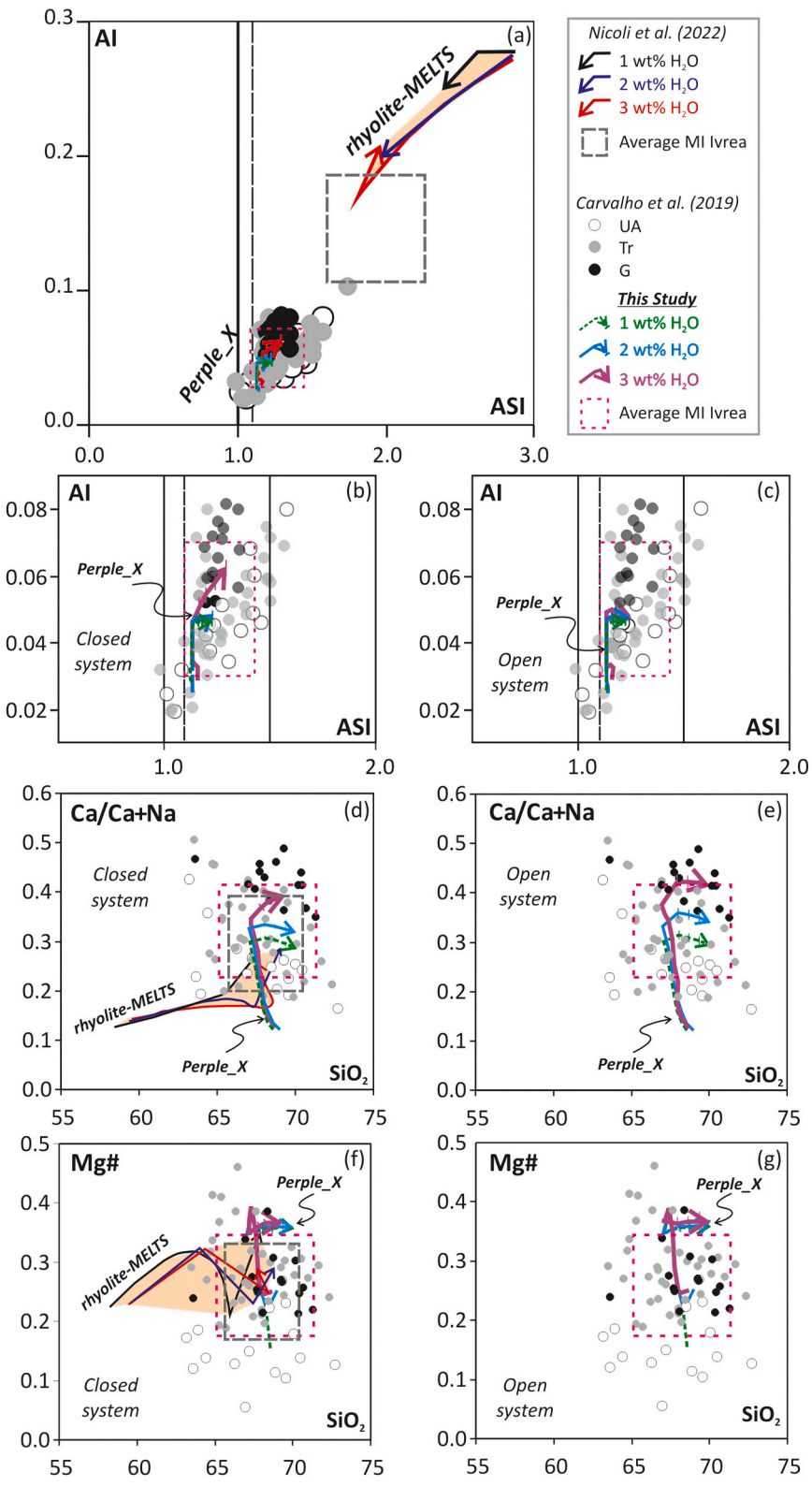

Fig. 9. Comparison between natural and calculated melt compositions. (a) Alkalinity index [AI = molar Al_2O_3 – (K_2O + Na_2O)] versus aluminium saturation index [ASI = molar Al_2O_3/(CaO + K_2O + Na_2O)] diagram containing NGs composition from Carvalho et al. (2019), model melts from rhyolite-MELTS (Nicoli et al., 2022) and Perple_X (this study). Gray dashed box: alleged average of IVZ NGs by Nicoli et al. (2022), does not overlap data from Carvalho et al. (2019) (pink dashed box). (b) and (c) AI vs. ASI close-up diagrams showing agreement between NGs (Carvalho et al., 2019), average NGs ± 1 sigma (pink dashed box) and model melts calculated using Perple_X under closed and open system, respectively. Decompression melting is represented by the steps in the arrows. (d) and (e) molar Ca/(Ca + Na) versus SiO_2 at closed and open system, respectively. (f) and (g) Mg# versus SiO_2 at closed and open system, respectively. UA = upper amphibolite facies, Tr = transition zone, G = granulite facies. (For interpretation of the references to colour in this figure legend, the reader is referred to the web version of this article.)

6.5. *Some problems with the use of experimental CO_2 and H_2O solubility data to interpret volatile budget of NGs*

The coexistence of C-bearing NGs and carbonic MFI in peritectic minerals of granulite facies rocks reflects a scenario of melt-fluid immiscibility during partial melting, where the anatectic melt was in equilibrium with a C–O–H fluid (Cesare et al., 2007). Under the assumption of negligible CH_4 solubility in rhyolitic melts, the C and H contents measured in re-homogenized NGs by NanoSIMS can be converted to CO_2 and H_2O, and the results compared with CO_2 solubility

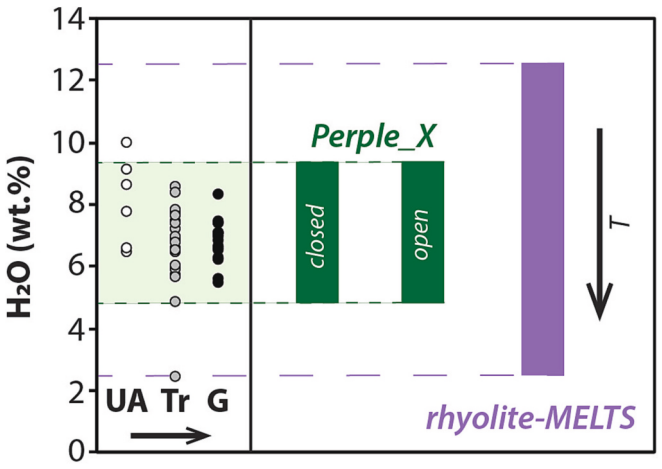

Fig. 10. H_2O (wt%) contents of re-homogenized NGs measured by NanoSIMS (Carvalho et al., 2019) and of model melts from Perple_X (this study) and rhyolite-MELTS (Nicoli et al., 2022). Black arrow indicates the increase in temperature for the calculated H_2O contents in the models. Size of data points correspond to one sigma error for each analysis.

data obtained from experimental studies. Such comparison is done in Fig. 11, considering the available experimental data for rhyolitic compositions (Fogel and Rutherford, 1990; Blank et al., 1993; Tamic et al., 2001; Duncan and Dasgupta, 2014, 2017) and anatectic melt inclusions (Carvalho et al., 2019; Gianola et al., 2020; Ferri et al., 2020; Ferrero et al., 2021; Borghini et al., 2023). The maximum CO_2 content of NGs increases with the pressure of formation, and to a lesser extent with temperature, in agreement with experimental results and model predictions (Fig. 11a,b). However, NGs show lower CO_2 contents than those predicted by experimentally determined CO_2 solubilities, at fixed pressure (Fig. 11a). On the other hand, temperature plays a more important role for H_2O, with melt inclusions generally showing higher values than experiments, at least at <1000 °C (Fig. 11d). A negative correlation between melt H_2O and pressure is shown by NGs between 0.5 and 1.0 GPa (Fig. 11c).

This comparison, however, requires a careful evaluation of how solubility experiments have been conducted. The majority of CO_2 solubility data available in the literature for rhyolitic compositions were determined from rhyolitic melts in equilibrium with a binary H_2O–CO_2 mixture or with only a CO_2 fluid, and never under graphite-saturated conditions (Fogel and Rutherford, 1990; Blank et al., 1993; Tamic et al., 2001; Duncan and Dasgupta, 2014; Muth et al., 2020). Graphite-bearing experiments were solely conducted by Duncan and Dasgupta (2017) and Yoshioka et al. (2019), the latter in equilibrium with a CO–CO_2 fluid phase. All the above experiments were run under (much) more oxidizing conditions than those occurring in graphitic systems at $X_O = 1/3$ (Connolly, 1995). Of course, solubility experiments conducted under very different oxygen fugacities and saturation conditions (for example, carbonate-saturated vs. graphite- and carbonate-saturated) result in different melt CO_2 solubilities, at fixed pressure, temperature and melt composition (black and white diamonds in Fig. 11). Therefore, it can be expected that CO_2 and H_2O solubilities determined under (highly) oxidizing conditions are maxima and minima, respectively, with little possibilities of extrapolation to the more reducing carbonate-free graphitic protoliths in which the CO_2 contents of melts seem to be lower. Moreover, some inconsistencies are also evident considering the experimental dataset. For example, Tamic et al. (2001) reported an increasing CO_2 content of melt with the increasing X_{CO2} fraction of the coexisting fluid at fixed pressure of 0.5 GPa, whereas the opposite trend is shown by the experimental melts of Duncan and Dasgupta (2014) at ≥1.5 GPa (Fig. 11). Such a mismatch is also present when H_2O of melt and X_{H2O} of fluid are considered (Fig. 11c). As a consequence, CO_2 solubility in rhyolitic melts is expected to decrease at increasing melt H_2O contents at low P conditions, whereas the opposite should occur at ≥1.5 GPa (Fig. 11).

From the results presented above we can conclude that the available CO_2 solubility experiments for rhyolitic compositions cannot be considered synthetic analogues of natural granulitic systems made of coexisting H_2O–CO_2–CH_4 ternary fluids, H_2O- and CO_2-bearing anatectic melts and graphite-bearing residues. Therefore, caution is also required in applying the CO_2 solubility models based on such experiments (e.g., Liu et al., 2005; Papale et al., 2006) to anatectic systems. Similarly, since the H_2O–CO_2 mixed fluid thermodynamic model developed for rhyolite-MELTS was calibrated on the basis of fluid saturation experiments involving H_2O, CO_2 and mixed H_2O–CO_2 fluid, using the experiments of Blank et al. (1993) and Tamic et al. (2001) for the rhyolite–H_2O–CO_2 system (Ghiorso and Gualda, 2015), this software may be unsuitable for tracking the volatile contents of melts produced by partial melting of graphitic metapelites. Even if Perple_X performs better at modelling melting equilibria of metasedimentary rocks, its application to graphitic systems still suffers from the lack of complete melt models accounting for C–O–H fluid species.

7. Implications and future research

In the crustal sequence of IVZ, anatectic melts and C–O–H fluids are present and coexist up to HT and, at least near UHT, conditions in graphitic metapelites, whereas the computational approach of Nicoli et al. (2022) predicted a limited extent (< 750 °C) of C–O–H fluid stability in the suprasolidus for the same rocks.

Natural evidence should be the benchmark for computational efforts, and at the present state of knowledge the modelling of suprasolidus graphitic metapelites is still far from satisfactory. A sound quantification of carbon budget and fluxes in suprasolidus graphitic metapelites should consider all the complex compositional relationships among fluid, melt and solids, as well as the possible respeciation in the fluid phases due to redox processes. In order to have a complete picture of carbon mobilization during crustal reworking, models must consider the persistence of C–O–H fluids in graphitic rocks such as those of the IVZ and, therefore, conditions of fluid-melt immiscibility up to near UHT conditions. Models should also conform to the natural evidence that the combined action of hydrous melt and C–O–H fluid is not able to dissolve and remove all the organic carbon in the metasedimentary crust. There is need for more data on graphitic anatectic systems, also to better constrain the possible internal origin of CO_2 by Fe^{3+} reduction during biotite melting (Cesare et al., 2005), as well as the impact of silicate dissolution on composition of C–O–H fluids (Tumiati et al., 2017) and the mutual relationships between fluid composition, solubility and respeciation. Similarly, future computational efforts should focus on popularizing a thermodynamic model of melt which includes at least CO_2 among the carbon species, functional for the most used software programs (e.g., Heinrich and Connolly, 2022). It is also essential to be able to model ternary H_2O–CO_2–CH_4 mixtures in the presence of melt and graphite, which demands targeted experimental studies.

Supplementary data to this article can be found online at https://doi.org/10.1016/j.chemgeo.2023.121503.

Declaration of Competing Interest

The authors have no financial or personal competing interests to declare.

Data availability

Data will be made available on request.

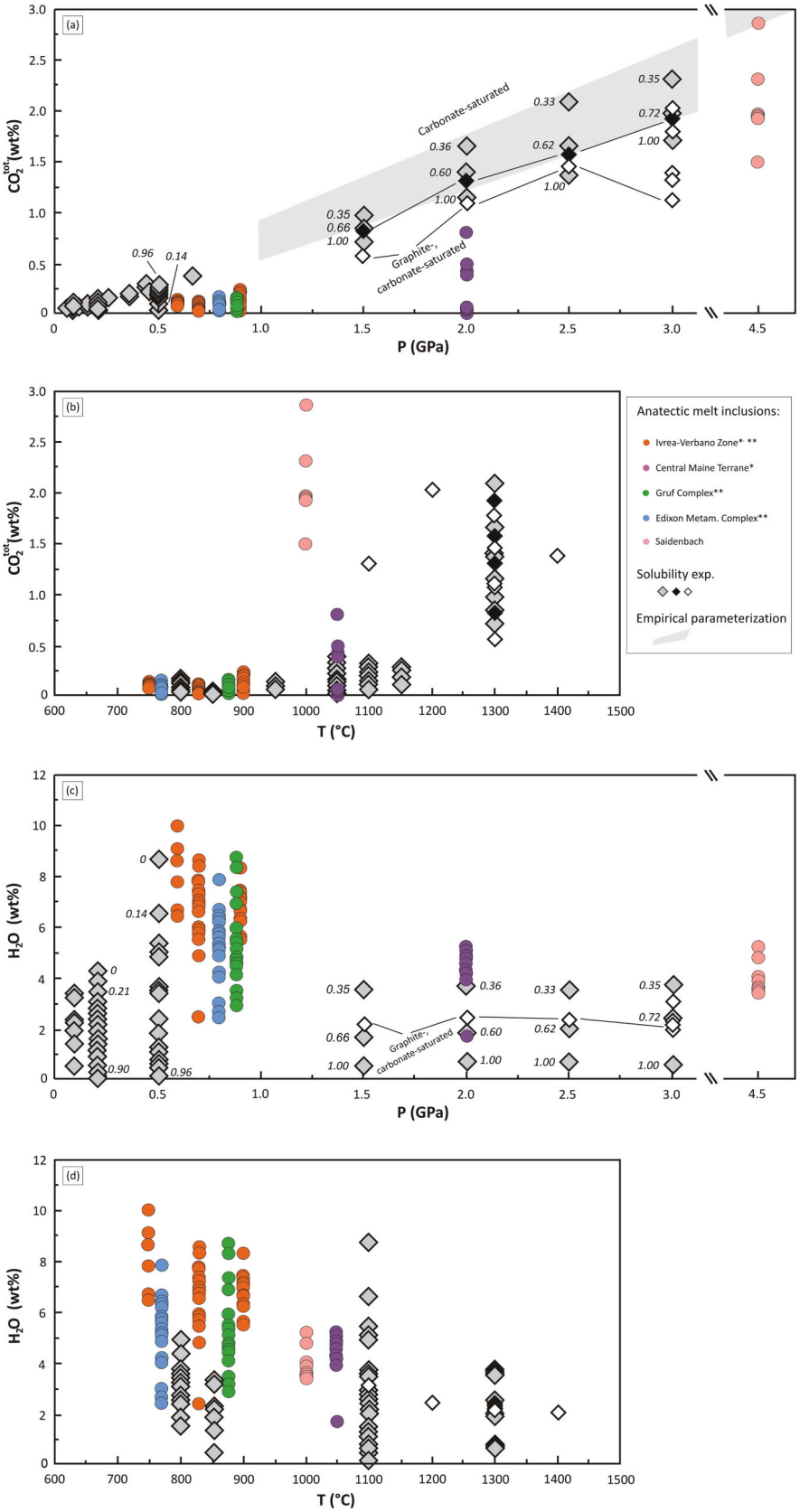

Fig. 11. Comparison between CO_2 and H_2O solubility data available for rhyolitic composition from the literature and CO_2 and H_2O contents measured in re-homogenized nanogranitoids and glassy melt inclusions. Experimental data at <1 GPa from Fogel and Rutherford (1990), Blank et al. (1993) and Tamic et al. (2001), at ≥1.5 GPa from Duncan and Dasgupta (2014, 2017). Italic values reflect the fraction of CO_2 in the fluid phase for experiments at 0.5 GPa (Tamic et al., 2001) and at 1.5–3.0 GPa (Duncan and Dasgupta, 2014). Melt inclusion data from Carvalho et al. (2019), Ferri et al. (2020), Ferrero et al. (2021), Gianola et al. (2021) and Borghini et al. (2023). Gray field represent predicted CO_2 at defined pressures calculated using the equation of Duncan and Dasgupta (2014) for 1 and 5 wt% H_2O. * = graphite-bearing; ** = NGs + MFIs. In figure (a) and (c), black lines connect experiments run at 1300 °C. Experiments of Fogel and Rutherford (1990) are not plotted in (c,d) because they consider only CO_2.

Acknowledgments

The authors acknoledge the following sources of funding: PNRA2018_103 and WelcomeKit to B.B.C., BART_SID19_01 to O.B., and MUR PRIN 2017ZE49E7 to B.C. O.B. acknowledges the support from the SIR Programme (Scientific Independence of young Researchers) of MIUR (Grant RBSI14Y7PF, "Carbon recycling during melting of the continental crust: implications for the long-term geochemical cycle"). Laszlo E. Aradi and Lisa Santello are thanked for their support during Raman analyses. We thank Nicoli et al. (2022) for prompting this paper by misreporting our previous work, and Jörg Hermann, Chris Yakymchuk and Balz Kamber who wisely conducted us in changing a comment into a more insightful manuscript.

References

Acosta-Vigil, A., London, D., G. B. M. VI, Cesare, B., Buick, I., Hermann, J., Bartoli, O., 2017. Primary crustal melt compositions: Insights into the controls, mechanisms and timing of generation from kinetics experiments and melt inclusions. Lithos 286, 454–479.

Ague, J.J., 1991. Evidence for major mass transfer and volume strain during regional metamorphism of pelites. Geology 19, 855–858.

Ague, J.J., Nicolescu, S., 2014. Carbon dioxide released from subduction zones by fluid-mediated reactions. Nat. Geosci. 7, 355–360.

Bakker, R.J., Jansen, J.B.H., 1991. Experimental post-entrapment water loss from synthetic CO2-H2O inclusions in natural quartz. Geochim. Cosmochim. Acta 55 (8), 2215–2230.

Barich, A., Acosta-Vigil, A., Garrido, C.J., Cesare, B., Tajčmanová, L., Bartoli, O., 2014. Microstructures and petrology of melt inclusions in the anatectic sequence of Jubrique (Betic Cordillera, S Spain): implications for crustal anatexis. Lithos 206, 303–320.

Bartoli, O., 2017. Phase equilibria modelling of residual migmatites and granulites: An evaluation of the melt-reintegration approach. J. Metamorph. Geol. 35, 919–942.

Bartoli, O., 2021. Characterizing fluid and melt in high-grade metamorphic rocks. In: Lecumberri-Sanchez, P., Steele-McInnis, M. (Eds.), Fluid Inclusions, Mineral Assoc Can, Short Course Ser, 49.

Bartoli, O., Carvalho, B.B., 2021. Anatectic granites in their source region: a comparison between experiments, thermodynamic modelling and nanogranitoids. Lithos 402, 106046.

Bartoli, O., Cesare, B., 2020. Nanorocks: a 10-year-old story. Rendiconti Lincei. Scienze Fisiche e Naturali 31, 249–257.

Bartoli, O., Cesare, B., Remusat, L., Acosta-Vigil, A., Poli, S., 2014. The H_2O content of granite embryos. Earth Planet. Sci. Lett. 395, 281–290.

Bea, F., Montero, P., 1999. Behavior of accessory phases and redistribution of Zr, REE, Y, Th, and U during metamorphism and partial melting of metapelites in the lower crust: an example from the Kinzigite Formation of Ivrea-Verbano, NW Italy. Geochim. Cosmochim. Acta 63, 1133–1153.

Behrens, H., Ohlhorst, S., Holtz, F., Champenois, M., 2004. CO2 solubility in dacitic melts equilibrated with H2O-CO2 fluids: implications for modeling the solubility of CO2 in silicic melts. Geochim. Cosmochim. Acta 68, 4687–4703.

Berkesi, M., Hidas, K., Guzmics, T., Dubessy, J., Bodnar, R.J., Szabó, C., Vajna, B., Tsunogae, T., 2009. Detection of small amounts of H2O in CO2–rich fluid inclusions using Raman spectroscopy. J. Raman Spectrosc. 40, 1461–1463.

Blank, J.G., Stolper, E.M., Carroll, M.R., 1993. Solubilities of carbon dioxide and water in rhyolitic melt at 850 C and 750 bars. Earth Planet. Sci. Lett. 119, 27–36.

Borghini, A., Nicoli, G., Ferrero, S., O'Brien, P.J., Laurent, O., Remusat, L., Borghini, G., Milani, S., 2023. The role of continental subduction in mantle metasomatism and carbon recycling revealed by melt inclusions in UHP eclogites. Sci. Adv. 9 eabp9482.

Brown, M., 2013. Granite: From genesis to emplacement. GSA Bull. 125, 1079–1113.

Carvalho, B.B., Sawyer, E.W., Janasi, V.D.A., 2016. Crustal reworking in a shear zone: transformation of metagranite to migmatite. J. Metamorph. Geol. 34, 237–264.

Carvalho, B.B., Bartoli, O., Ferri, F., Cesare, B., Ferrero, S., Remusat, L., Poli, S., 2019. Anatexis and fluid regime of the deep continental crust: New clues from melt and fluid inclusions in metapelitic migmatites from Ivrea Zone (NW Italy). J. Metamorph. Geol. 37, 951–975.

Carvalho, B.B., Bartoli, O., Cesare, B., Tacchetto, T., Gianola, O., Ferri, F., Szabó, C., 2020. Primary CO2-bearing fluid inclusions in granulitic garnet usually do not survive. Earth Planet. Sci. Lett. 536, 116170.

Cesare, B., 1995. Graphite precipitation in C—O—H fluid inclusions: closed system compositional and density changes, and thermobarometric implications. Contrib. Mineral. Petrol. 122 (1-2), 25–33.

Cesare, B., Meli, S., Nodari, L., Russo, U., 2005. Fe^{3+} reduction during biotite melting in graphitic metapelites: another origin of CO2 in granulites. Contrib. Mineral. Petrol. 149, 129–140.

Cesare, B., Maineri, C., Toaldo, A.B., Pedron, D., Acosta-Vigil, A., 2007. Immiscibility between carbonic fluids and granitic melts during crustal anatexis: a fluid and melt inclusion study in the enclaves of the Neogene Volcanic Province of SE Spain. Chem. Geol. 237, 433–449.

Cesare, B., Ferrero, S., Salvioli-Mariani, E., Pedron, D., Cavallo, A., 2009. "Nanogranite" and glassy inclusions: The anatectic melt in migmatites and granulites. Geology 37, 627–630.

Cesare, B., Acosta-Vigil, A., Bartoli, O., Ferrero, S., 2015. What can we learn from melt inclusions in migmatites and granulites? Lithos 239, 186–216.

Chu, X., Ague, J.J., 2013. Phase equilibria for graphitic metapelite including solution of CO 2 in melt and cordierite: implications for dehydration, partial melting and graphite precipitation. J. Metamorph. Geol. 31, 843–862.

Coggon, R., Holland, T.J.B., 2002. Mixing properties of phengitic micas and revised garnet-phengite thermobarometers. J. Metamorph. Geol. 20, 683–696.

Connolly, J.A.D., 1995. Phase diagram methods for graphitic rocks and application to the system C− O− H− FeO− TiO2− SiO2. Contrib. Mineral. Petrol. 119, 94–116.

Connolly, J.A.D., 2009. The geodynamic equation of state: what and how. Geochem. Geophys. Geosyst. 10.

Connolly, J.A.D., Cesare, B., 1993. C-O-H-S fluid composition and oxygen fugacity in graphitic metapelites. J. Metamorph. Geol. 11, 379–388.

Dasgupta, R., Hirschmann, M.M., 2010. The deep carbon cycle and melting in Earth's interior. Earth Planet. Sci. Lett. 298, 1–13.

Dubessy, J., Poty, B., Ramboz, C., 1989. Advances in COHNS fluid geochemistry based on micro-Raman spectrometric analysis of fluid inclusions. Eur. J. Mineral. 517–534.

Duncan, M.S., Dasgupta, R., 2014. CO_2 solubility and speciation in rhyolitic sediment partial melts at 1.5–3.0 GPa–implications for carbon flux in subduction zones. Geochim. Cosmochim. Acta 124, 328–347.

Duncan, M.S., Dasgupta, R., 2017. Rise of Earth's atmospheric oxygen controlled by efficient subduction of organic carbon. Nat. Geosci. 10, 387–392.

Epstein, G.S., Bebout, G.E., Angiboust, S., Agard, P., 2020. Scales of fluid-rock interaction and carbon mobility in the deeply underplated and HP-Metamorphosed Schistes Lustrés, Western Alps. Lithos 354, 105229.

Ewing, T.A., Hermann, J., Rubatto, D., 2013. The robustness of the Zr-in-rutile and Ti-in-zircon thermometers during high-temperature metamorphism (Ivrea-Verbano Zone, northern Italy). Contrib. Mineral. Petrol. 165, 757–779.

Ferrero, S., Bodnar, R.J., Cesare, B., Viti, C., 2011. Re-equilibration of primary fluid inclusions in peritectic garnet from metapelitic enclaves, El Hoyazo, Spain. Lithos 124, 117–131.

Ferrero, S., Braga, R., Berkesi, M., Cesare, B., Laridhi Ouazaa, N., 2014. Production of metaluminous melt during fluid-present anatexis: an example from the Maghrebian basement, La Galite Archipelago, central Mediterranean. J. Metamorph. Geol. 32, 209–225.

Ferrero, S., O'Brien, P.J., Borghini, A., Wunder, B., Wälle, M., Günter, C., Ziemann, M.A., 2019. A treasure chest full of nanogranitoids: an archive to investigate crustal melting in the Bohemian Massif. Geol. Soc. Lond., Spec. Publ. 478, 13–38.

Ferrero, S., Ague, J.J., O'Brien, P.J., Wunder, B., Remusat, L., Ziemann, M.A., Axler, J., 2021. High-pressure, halogen-bearing melt preserved in ultrahigh-temperature felsic granulites of the Central Maine Terrane, Connecticut (USA). Am. Mineral. 106, 1225–1236.

Ferri, F., Gibert, B., Violay, M., Cesare, B., 2013. Electrical conductivity in a partially molten crust from measurements on metasedimentary enclaves. Tectonophysics 586, 84–94.

Ferri, F., Burlini, L., Cesare, B., 2016. Effect of partial melting on Vp and Vs in crustal enclaves from Mazarrón (SE Spain). Tectonophysics 671, 139–150.

Ferri, F., Cesare, B., Bartoli, O., Ferrero, S., Palmeri, R., Remusat, L., Poli, S., 2020. Melt inclusions at MT. Edixon (Antarctica): chemistry, petrology and implications for the evolution of the Lanterman range. Lithos 374, 105685.

Fogel, R.A., Rutherford, M.J., 1990. The solubility of carbon dioxide in rhyolitic melts; a quantitative FTIR study. Am. Mineral. 75, 1311–1326.

Frezzotti, M.L., Selverstone, J., Sharp, Z.D., Compagnoni, R., 2011. Carbonate dissolution during subduction revealed by diamond-bearing rocks from the Alps. Nat. Geosci. 4, 703–706.

Frezzotti, M.L., Ferrando, S., Tecce, F., Castelli, D., 2012a. Water content and nature of solutes in shallow-mantle fluids from fluid inclusions. Earth Planet. Sc. Lett. 351, 70–83.

Frezzotti, M.L., Tecce, F., Casagli, A., 2012b. Raman spectroscopy for fluid inclusion analysis. J. Geochem. Explor. 112, 1–20.

Gao, P., Zheng, Y.F., Zhao, Z.F., 2016. Experimental melts from crustal rocks: a lithochemical constraint on granite petrogenesis. Lithos 266, 133–157.

Gardner, J.E., Befus, K.S., Gualda, G.A., Ghiorso, M.S., 2014. Experimental constraints on rhyolite-MELTS and the Late Bishop Tuff magma body. Contrib. Mineral. Petrol. 168, 1–14.

Gervais, F., Trapy, P.H., 2021. Testing solution models for phase equilibrium (forward) modeling of partial melting experiments. Contrib. Mineral. Petrol. 176, 4.

Gerya, T.V., Meilick, F.I., 2011. Geodynamic regimes of subduction under an active margin: effects of rheological weakening by fluids and melts. J. Metamorph. Geol. 29, 7–31.

Ghiorso, M.S., Gualda, G.A., 2015. An H2O–CO2 mixed fluid saturation model compatible with rhyolite-MELTS. Contrib. Mineral. Petrol. 169, 1–30.

Gianola, O., Bartoli, O., Ferri, F., Galli, A., Ferrero, S., Capizzi, L.S., Liebske, C., Remusat, L., Poli, S., Cesare, B., 2021. Anatectic melt inclusions in ultra high temperature granulites. J. Metamorph. Geol. 39 (3), 321–342.

Groppo, C., Rapa, G., Frezzotti, M.L., Rolfo, F., 2021. The fate of calcareous pelites in collisional orogens. J. Metamorph. Geol. 39 (2), 181–207.

Groppo, C., Rolfo, F., Frezzotti, M.L., 2022. CO_2 outgassing during collisional orogeny is facilitated by the generation of immiscible fluids. Commun. Earth Environ. 3, 1–11.

Gualda, G.A., Ghiorso, M.S., Lemons, R.V., Carley, T.L., 2012. Rhyolite-MELTS: a modified calibration of MELTS optimized for silica-rich, fluid-bearing magmatic systems. J. Petrol. 53, 875–890.

Guo, S., Hermann, J., Tang, P., Chu, X., Chen, Y., Su, B., 2022. Formation of carbon-bearing silicate melts by melt-metacarbonate interaction at convergent plate margins. Earth Planet. Sci. Lett. 597, 117816.

Hacker, B.R., Kelemen, P.B., Behn, M.D., 2015. Continental lower crust. Annu. Rev. Earth Planet. Sci. 43, 167–205.
Harley, S.L., 2004. Extending our understanding of ultrahigh temperature crustal metamorphism. J. Mineral. Petrol. Sci. 99, 140–158.
Harlov, D.E., Förster, H.J., 2002. High-grade fluid metasomatism on both a local and a regional scale: the Seward peninsula, Alaska, and the Val Strona di Omegna, Ivrea–Verbano Zone, Northern Italy. Part I: petrography and silicate mineral chemistry. J. Petrol. 43, 769–799.
Heinrich, C.A., Connolly, J.A., 2022. Physical transport of magmatic sulfides promotes copper enrichment in hydrothermal ore fluids. Geology 50, 1101–1105.
Hernández-Uribe, D., Spera, F.J., Bohrson, W.A., Heinonen, J.S., 2022. A comparative study of two-phase equilibria modeling tools: MORB equilibrium states at variable pressure and H2O concentrations. Am. Mineral. 107, 1789–1806.
Holland, T.J.B., Powell, R.T.J.B., 1998. An internally consistent thermodynamic data set for phases of petrological interest. J. Metamorph. Geol. 16, 309–343.
Holland, T., Powell, R., 2003. Activity–composition relations for phases in petrological calculations: an asymmetric multicomponent formulation. Contrib. Mineral. Petrol. 145, 492–501.
Holland, T.J.B., Powell, R., 2011. An improved and extended internally consistent thermodynamic dataset for phases of petrological interest, involving a new equation of state for solids. J. Metamorph. Geol. 29, 333–383.
Huizenga, J.M., Touret, J.L., 2012. Granulites, CO_2 and graphite. Gondwana Res. 22, 799–809.
Johannes, W., Holtz, F., 1990. Formation and composition of H 2 O-undersaturated granitic melts. In: High-temperature metamorphism and crustal anatexis. Springer, Dordrecht, pp. 87–104.
Johnson, T., Yakymchuk, C., Brown, M., 2021. Crustal melting and suprasolidus phase equilibria: from first principles to the state-of-the-art. Earth Sci. Rev. 221, 103778.
Kelemen, P.B., Manning, C.E., 2015. Reevaluating carbon fluxes in subduction zones, what goes down, mostly comes up. Proc. Natl. Acad. Sci. 112, E3997–E4006.
Kohn, M.J., 2020. A refined zirconium-in-rutile thermometer. Am. Mineral. 105, 963–971.
Kunz, B.E., White, R.W., 2019. Phase equilibrium modelling of the amphibolite to granulite facies transition in metabasic rocks (Ivrea Zone, NW Italy). J. Metamorph. Geol. 37, 935–950.
Lamadrid, H.M., Lamb, W.M., Santosh, M., Bodnar, R.J., 2014. Raman spectroscopic characterization of H2O in CO2-rich fluid inclusions in granulite facies metamorphic rocks. Gondwana Res. 26, 301–310.
Li, S., Li, J., Chou, I.M., Jiang, L., Ding, X., 2017. The formation of the Yichun Ta-Nb deposit, South China, through fractional crystallization of magma indicated by fluid and silicate melt inclusions. J. Asian Earth Sci. 137, 180–193.
Liu, Y., Zhang, Y., Behrens, H., 2005. Solubility of H2O in rhyolitic melts at low pressures and a new empirical model for mixed H2O–CO2 solubility in rhyolitic melts. J. Volcanol. Geotherm. Res. 143, 219–235.
Luvizotto, G.L., Zack, T., 2009. Nb and Zr behavior in rutile during high-grade metamorphism and retrogression: an example from the Ivrea–Verbano Zone. Chem. Geol. 261, 303–317.
Maffeis, A., Ferrando, S., Connolly, J.A., Groppo, C., Frezzotti, M.L., Castelli, D., 2021. Thermodynamic analysis of HP-UHP fluid inclusions: The solute load and chemistry of metamorphic fluids. Geochim. Cosmochim. Acta 315, 207–229.
Martin, L.A., Hermann, J., 2018. Experimental phase relations in altered oceanic crust: implications for carbon recycling at subduction zones. J. Petrol. 59, 299–320.
Muth, M., Duncan, M.S., Dasgupta, R., 2020. The effect of variable Na/K on the CO2 content of slab-derived rhyolitic melts. In: Carbon in Earth's Interior, pp. 195–208.
Mysen, B.O., Fogel, M.L., Morrill, P.L., Cody, G.D., 2009. Solution behavior of reduced COH volatiles in silicate melts at high pressure and temperature. Geochim. Cosmochim. Acta 73, 1696–1710.
Nestola, F., Korolev, N., Kopylova, M., Rotiroti, N., Pearson, D.G., Pamato, M.G., Alvaro, M., Peruzzo, L., Gurney, J.J., Moore, A.E., Davidson, J., 2018. CaSiO3 perovskite in diamond indicates the recycling of oceanic crust into the lower mantle. Nature 555, 237–241.
Newton, R.C., Charlu, T.V., Kleppa, O.J., 1980a. Thermochemistry of the high structural state plagioclases. Geochim. Cosmochim. Acta 44 (7), 933–941.
Newton, R.C., Smith, J.V., Windley, B.F., 1980b. Carbonic metamorphism, granulites and crustal growth. Nature 288, 45–50.
Nicoli, G., Borghini, A., Ferrero, S., 2022. The carbon budget of crustal reworking during continental collision: clues from nanorocks and fluid inclusions. Chem. Geol. 608, 121025.
Papale, P., Moretti, R., Barbato, D., 2006. The compositional dependence of the saturation surface of H2O+ CO2 fluids in silicate melts. Chem. Geol. 229, 78–95.
Pape, J., Mezger, K., Robyr, M., 2016. A systematic evaluation of the Zr-in-rutile thermometer in ultra-high temperature (UHT) rocks. Contrib. Mineral. Petrol. 171, 1–20.
Patiño Douce, A.E., Johnston, A.D., 1991. Phase equilibria and melt productivity in the pelitic system: implications for the origin of peraluminous granitoids and aluminous granulites. Contrib. Mineral. Petrol. 107, 202–218.
Peterson, J.W., Chacko, T., Kuehner, S.M., 1991. The effects of fluorine on the vapor-absent melting of phlogopite+ quartz: implications for deep-crustal processes. Am. Mineral. 76, 470–476.
Plank, T., Manning, C.E., 2019. Subducting carbon. Nature 574, 343–352.
Poli, S., 2015. Carbon mobilized at shallow depths in subduction zones by carbonatitic liquids. Nat. Geosci. 8, 633–636.
Quick, J.E., Sinigoi, S., Snoke, A.W., Kalakay, T.J., Mayer, A., Peressini, G., 2003. Geologic map of the southern Ivrea-Verbano Zone, northwestern Italy. US Geol. Survey, I-Map 2776.
Redler, C., Johnson, T.E., White, R.W., Kunz, B.E., 2012. Phase equilibrium constraints on a deep crustal metamorphic field gradient: metapelitic rocks from the Ivrea Zone (NW Italy). J. Metamorph. Geol. 30, 235–254.
Redler, C., White, R.W., Johnson, T.E., 2013. Migmatites in the Ivrea Zone (NW Italy): constraints on partial melting and melt loss in metasedimentary rocks from Val Strona di Omegna. Lithos 175, 40–53.
Roedder, E., 1984. Volume 12: fluid inclusions. Mineral. Soc. Am. 12.
Rudnick, R.L., Fountain, D.M., 1995. Nature and composition of the continental crust: a lower crustal perspective. Rev. Geophys. 33, 267–309.
Safonov, O.G., Mityaev, A.S., Yapaskurt, V.O., Belyanin, G.A., Elburg, M., Rajesh, H.M., Smit, A.C., 2020. Carbonate-silicate inclusions in garnet as evidence for a carbonate-bearing source for fluids in leucocratic granitoids associated with granulites of the Southern Marginal Zone, Limpopo Complex, South Africa. Gondwana Res. 77, 147–167.
Sarkar, S., Santosh, M., Dasgupta, S., Fukuoka, M., 2003. Very high density CO2 associated with ultrahigh-temperature metamorphism in the Eastern Ghats granulite belt, India. Geology 31, 51–54.
Scambelluri, M., Cannaò, E., Guerini, S., Bebout, G.E., Epstein, G., Rotondo, F., Campomenosi, N., Tartarotti, P., 2022. Carbon mobility and exchange in a plate-interface subduction mélange: a case study of meta-ophiolitic rocks in Champorcher Valley, Italian Alps. Lithos 428–429, 106813.
Schmid, R., 1968. Schwierigkeiten der Nomenldatur und Klassifikation massiger Katametamorphite, erlautert am Beispiel der Zone Ivrea-Verbano (Norditalien). Schweiz. Mineral. Petrogr. Mitt. 48, 81–90.
Schmid, S.M., 1993. Ivrea zone and adjacent southern Alpine basement. In: Raumer, J.F., Neubauer, F. (Eds.), Pre-Mesozoic Geology in the Alps. Springer Verlag, Berlin, pp. 567–583.
Schmid, R., Wood, B.J., 1976. Phase relationships in granulitic metapelites from the Ivrea-Verbano zone (Northern Italy). Contrib. Mineral. Petrol. 54, 255–279.
Spránitz, T., Padrón-Navarta, J.A., Szabó, C., Szabó, Á., Berkesi, M., 2022. Abiotic passive nitrogen and methane enrichment during exhumation of subducted rocks: primary multiphase fluid inclusions in high-pressure rocks from the Cabo Ortegal Complex, NW Spain. J. Metamorph. Geol. 40, 1291–1319.
Stewart, E.M., Ague, J.J., 2020. Pervasive subduction zone devolatilization recycles CO2 into the forearc. Nat. Commun. 11, 1–8.
Tacchetto, T., Bartoli, O., Cesare, B., Berkesi, M., Aradi, L.E., Dumond, G., Szabó, C., 2019. Multiphase inclusions in peritectic garnet from granulites of the Athabasca granulite terrane (Canada): Evidence of carbon recycling during Neoarchean crustal melting. Chem. Geol. 508, 197–209.
Tajčmanová, L., Connolly, J.A.D., Cesare, B., 2009. A thermodynamic model for titanium and ferric iron solution in biotite. J. Metamorph. Geol. 27, 153–165.
Tamic, N., Behrens, H., Holtz, F., 2001. The solubility of H2O and CO2 in rhyolitic melts in equilibrium with a mixed CO2–H2O fluid phase. Chem. Geol. 174, 333–347.
Thompson, J.B., Hovis, G.L., 1979. Entropy of mixing in sanidine. Am. Mineral. 64, 57–65.
Touret, J., 1971. Le facies granulite en Norvege Meridionale: II. Les inclusions fluides. Lithos 4, 423–436.
Touret, J.L., Huizenga, J.M., 2012. Fluid-assisted granulite metamorphism: a continental journey. Gondwana Res. 21, 224–235.
Tumiati, S., Tiraboschi, C., Sverjensky, D.A., Pettke, T., Recchia, S., Ulmer, P., Poli, S., 2017. Silicate dissolution boosts the CO2 concentrations in subduction fluids. Nat. Commun. 8 (1), 1–11.
Van den Kerkhof, A.M., Olsen, S.N., 1990. A natural example of superdense CO2 inclusions: microthermometry and Raman analysis. Geochim. Cosmochim. Acta 54, 895–901.
Vitale Brovarone, A., Martinez, I., Elmaleh, A., Compagnoni, R., Chaduteau, C., Ferraris, C., Esteve, I., 2017. Massive production of abiotic methane during subduction evidenced in metamorphosed ophicarbonates from the Italian Alps. Nat. Commun. 8, 1–13.
Wang, X., Chou, I.M., Hu, W., Burruss, R.C., Sun, Q., Song, Y., 2011. Raman spectroscopic measurements of CO2 density: Experimental calibration with high-pressure optical cell (HPOC) and fused silica capillary capsule (FSCC) with application to fluid inclusion observations. Geochim. Cosmochim. Acta 75, 4080–4093.
Wang, G., Thybo, H., Artemieva, I.M., 2021. No mafic layer in 80 km thick Tibetan crust. Nat. Commun. 12, 1–9.
White, R.W., Powell, R., Holland, T.J.B., Worley, B.A., 2000. The effect of TiO2 and Fe2O3 on metapelitic assemblages at greenschist and amphibolite facies conditions: mineral equilibria calculations in the system K2O–FeO–MgO–Al2O3–SiO2–H2O–TiO2–Fe2O3. J. Metamorph. Geol. 18, 497–511.
White, R.W., Powell, R., Holland, T.J.B., 2007. Progress relating to calculation of partial melting equilibria for metapelites. J. Metamorph. Geol. 25, 511–527.
White, R.W., Powell, R., Holland, T.J.B., Johnson, T.E., Green, E.C.R., 2014a. New mineral activity–composition relations for thermodynamic calculations in metapelitic systems. J. Metamorph. Geol. 32, 261–286.
White, R.W., Powell, R., Johnson, T.E., 2014b. The effect of Mn on mineral stability in metapelites revisited: new a–x relations for manganese-bearing minerals. J. Metamorph. Geol. 32, 809–828.

Yang, L., Miller, C.F., Wu, F.Y., 2022. Estimating crystallization pressure of peraluminous melts: an experimentally based empirical approach. Contrib. Mineral. Petrol. 177, 1–17.
Yoshioka, T., Nakashima, D., Nakamura, T., Shcheka, S., Keppler, H., 2019. Carbon solubility in silicate melts in equilibrium with a CO-CO2 gas phase and graphite. Geochim. Cosmochim. Acta 259, 129–143.
Zhang, X.S., Xu, X.S., Xia, Y., Zhao, K., 2021. Crystallization and melt extraction of a garnet-bearing charnockite from South China: Constraints from petrography, geochemistry, mineral thermometry, and rhyolite-MELTS modeling. Am. Mineral. 106, 461–480.